

AD-A179 383



DTIC  
ELECT  
APR 17 1987

S D

THE CHARACTERIZATION OF WHISKERS  
PRODUCED BY ELECTROMIGRATION ON  
SUSPENDED ALUMINUM LINESTRIPES

THESIS

Scott L. Linder  
Captain, USAF

**DISTRIBUTION STATEMENT A**

Approved for public release;  
Distribution Unlimited

DEPARTMENT OF THE AIR FORCE  
AIR UNIVERSITY

**AIR FORCE INSTITUTE OF TECHNOLOGY**

Wright-Patterson Air Force Base, Ohio

PII Redacted

87 4 16 037

1

SECRET  
APR 17 1987  
D

THE CHARACTERIZATION OF WHISKERS  
PRODUCED BY ELECTROMIGRATION ON  
SUSPENDED ALUMINUM LINESTRIPES

THESIS

Scott L. Linder  
Captain, USAF

AFIT/GE/ENG/86D-35

DISTRIBUTION STATEMENT A  
Approved for public release;  
Distribution Unlimited

THE CHARACTERIZATION OF WHISKERS  
PRODUCED BY ELECTROMIGRATION ON  
SUSPENDED ALUMINUM LINESTRIPES

THESIS

Presented to the Faculty of the School of Engineering  
of the Air Force Institute of Technology  
Air University  
In Partial Fulfillment of the  
Requirements for the Degree of  
Master of Science in Electrical Engineering



Scott L. Linder, B.S.  
Captain, USAF

December 1986

Accession For	
NTIS CRA&I	<input checked="checked" type="checkbox"/>
DTIC TAB	<input type="checkbox"/>
Unannounced	<input type="checkbox"/>
Justification	
By	
Distribution/	
Availability Codes	
Dist	Avail and/or Special
A-1	

## Preface

The purpose of this study was to determine the crystallographic orientation of aluminum whiskers produced by electromigration. The analysis was performed using scanning transmission electron microscopy. The importance of this study lies in the threat posed by whiskers to the reliability of Very Large Scale Integrated (VLSI) circuits and Very High Speed Integrated Circuits (VHSIC).

I would like to express thanks to all of those whose contributions were vital to this research. A special thank-you goes to my advisor, Major Donald R. Kitchen, for his expertise, direction, and persistence in keeping me on track. Sincere appreciation is also extended to the readers on my thesis committee, Major Ed Kolesar and Capt Randy Jost, for their insight and suggestions. A deep appreciation is extended to the team from System Research Laboratories (SRL): Mr. Ralph Omlar for his time and effort in operating the scanning transmission electron microscope (STEM), Ms. Pam Lloyd for her help with the STEM and ion milling, Ms. Cheryl Heidelberg and Mr. Scott Apt for photographic assistance, and Mr. Rick Bacon and Mr. Bob Burdecki for their assistance with the scanning electron microscopes (SEM). I would like to thank Mr. William Anderson of the Air Force Wright Aeronautical Laboratories for his work with the SEM.

Appreciation is also extended to Mr. Don Smith and Mr.

Larry Calahan for their technical assistance in fabrication and packaging.

Finally, a very special thanks goes to my wife, Angela Linder, and my children Stacey and Sarah Linder, for their continued support and understanding throughout my AFIT tour.

Scott L. Linder

## Table of Contents

	Page
Preface.....	i
List of Figures.....	v
Abstract.....	viii
I. Introduction.....	I-1
Problem Statement.....	I-1
Major Results.....	I-2
Assumptions.....	I-3
Scope.....	I-3
General Approach.....	I-4
Major Equipment Used.....	I-5
Sequence of Presentation.....	I-5
II. Background.....	II-1
Electromigration Theory.....	II-2
Potential Well Model.....	II-2
Ballistic Model.....	II-4
Composition Gradients.....	II-9
Temperature Gradients.....	II-11
Compressive Stress.....	II-13
Stress Due to Temperature.....	II-14
Stress Due to Electromigration.....	II-14
Thermally Produced Whiskers.....	II-18
Role of Compressive Stress.....	II-19
Nucleation Sites.....	II-19
Whisker Orientation and Morphology.....	II-20
Previous TEM Insitu Electromigration Experiments .....	II-21
Summary.....	II-24
III. Experimental Equipment and Procedures.....	III-1
Test Pattern.....	III-1
Test Equipment.....	III-3
Test Station.....	III-3
Mark II Holder.....	III-6
Vacuum Box.....	III-7
Electron Microscopes.....	III-8
Testing Procedures.....	III-9
Static Testing.....	III-9
Sample Preparation.....	III-9
Powered Test.....	III-12
Insitu Testing.....	III-13
Sample Preparation.....	III-14
Powered Test.....	III-16

Whisker Analysis Procedures.....	III-16
Inspection.....	III-16
Bright Field Micrographs.....	III-17
Diffraction Patterns.....	III-17
Dark Field Micrographs.....	III-17
SEM Micrographs.....	III-18
Insitu Observation Techniques.....	III-18
Summary.....	III-19
IV. Results and Discussion.....	IV-1
Electromigration.....	IV-1
Results of Whisker Analysis.....	IV-4
Crystallographic Orientation.....	IV-7
Spot Pattern Analysis.....	IV-14
Calibration of Al Diffraction Rings....	IV-14
Ratio Test.....	IV-16
Mapping the Spot Pattern.....	IV-17
Determining the Orientation of the	
Whisker.....	IV-20
Orientation Results.....	IV-21
Morphology.....	IV-21
Internal Structure.....	IV-21
Shape/Striations.....	IV-23
Kinking.....	IV-24
Nucleation Sites.....	IV-25
Short Circuit.....	IV-27
Summary.....	IV-28
V. Conclusions and Recommendations.....	V-1
Conclusions.....	V-1
Recommendations.....	V-2
Test Improvements.....	V-2
New Research.....	V-3
Appendix A Test Pattern Fabrication.....	A-1
Appendix B Producing Suspended Linestripes.....	B-1
Appendix C Thermal Model of a Suspended Linestripe..	C-1
Appendix D AC Tests.....	D-1
Bibliography.....	BIB-1
Vita.....	VITA-1

## List of Figures

Figure	Page
2.1 Model for Vacancy Diffusion.....	II-3
2.2 Forces Acting on an Ion at Its Saddle Point .....	II-5
2.3 Grain Boundary Representations.....	II-10
2.4 Depletion/Accumulation at Triple Points.....	II-10
2.5 Heat Flow From Aluminum Stripe to Ground Plate.....	II-12
2.6 Average Drift Velocity vs Current Density.....	II-16
2.7 Effective Length Reduced by Narrow Stripes.....	II-17
2.8 Observed Whisker Base Morphology for Thermally Grown Whiskers.....	II-20
3.1 Bridge Test Vehicle.....	III-2
3.2 Block Diagram of the Test Station.....	III-4
3.3 Timer.....	III-4
3.4 Mark II Holder with Bonded Test Sample.....	III-6
3.5 Bonding Pads Identified by Color Coded Connections.....	III-7
3.6 Vacuum Box.....	III-8
3.7 Etched Sample Mounted and Bonded to a TO-5 Header.....	III-10
3.8 BTV Mounted to a Copper Bulk Holder After Static Testing.....	III-14
3.9 Sample Bonded to the Mark II Holder.....	III-15
4.1 Observation of Increased Electromigration in Longer Stripes.....	IV-3
4.2 SEM Micrographs of Whisker #1 - #6.....	IV-5
4.3 SEM Micrographs of Whisker #7 - #12.....	IV-6



4.4	Bright Field and Dark Field Micrographs of Whisker #1.....	IV-8
4.5	Double Exposure of Spot Pattern and Bright Field Micrograph for Whisker #1.....	IV-9
4.6	Double Exposure of Spot Pattern and Bright Field Micrograph for Whisker #2.....	IV-10
4.7	Double Exposure of Spot Pattern and Bright Field Micrograph for Whisker #3.....	IV-11
4.8	Double Exposure of Spot Pattern and Bright Field Micrograph for Whisker #4.....	IV-12
4.9	Double Exposure of Spot Pattern and Bright Field Micrograph for Whisker #8.....	IV-13
4.10	Diffraction Pattern Produced By Aluminum Standard.....	IV-14
4.11	Diffraction Patterns of the Al Standard at 100 KV and Test Stripe at 200 KV.....	IV-16
4.12	Mapping of Spot Patterns for Whisker #1.....	IV-18
4.13	Pre-Mapped Spot Pattern.....	IV-19
4.14	Spot Pattern With the Whisker Axis Indicated by an Arrow.....	IV-20
4.15	Bright Field Micrograph of Whisker #2 Depicting Internal Dislocations.....	IV-22
4.16	Cross Sectional View of Whisker #1.....	IV-23
4.17	Kinking in Whisker #9.....	IV-24
4.18	SEM Micrograph of the Swollen Base Around Whisker #8.....	IV-26
4.19	Bright Field Micrograph of Whisker #8.....	IV-26
4.20	The Remains of Whisker #3 After Creating a Short Circuit With an Adjacent Stripe.....	IV-27
A.1	Lift-off Technique.....	A-4
C.1	Maximum Temperature at the Center of the Stripe for $J = 0.5 \times 10^6 \text{ A/cm}^2$ .....	C-3

C.2	Normalized Thermal Profile for a Suspended Linestripe.....	C-4
C.3	Maximum Temperature Gradient as a Function of Length for $J = 0.5 \times 10^6$ A/cm <sup>2</sup> .....	C-5
C.4	Normalized Graph of the Temperature Gradient for Suspended Linestripes.....	C-6
C.5	Thermal Conductance Model.....	C-6
D.1	AC Test Equipment.....	D-2
D.2	Thermal Migration .....	D-4

Abstract

Studies have shown that aluminum whiskers resulting from electromigration are as threatening to device reliability as void formation. ~~However~~, comparatively little research has been conducted to study their morphology or formation. This study generates whiskers on suspended aluminum test stripes. The aluminum is evaporated onto 9 mil thick silicon wafers with a 5000 Å layer of thermally grown silicon dioxide. Normal photolithography techniques are used to produce serpentine test patterns. The silicon substrate is chemically etched to produce aluminum stripes suspended on a thin layer of silicon dioxide. A current density of approximately  $450000 \text{ A/cm}^2$  is applied to induce electromigration. The whiskers are examined with a Cambridge MK II Scanning Electron Microscope and analyzed with a JEOL 2000FX Scanning Transmission Electron Microscope. The results of the analysis show that aluminum whiskers grow in a  $\langle 110 \rangle$  direction along the crystal axis. Additional morphological observations reveal internal dislocations and mass accumulation beneath the stripe surface at the whisker's nucleation site. (The ...)

THE CHARACTERIZATION OF WHISKERS  
PRODUCED BY ELECTROMIGRATION ON  
SUSPENDED ALUMINUM LINESTRIPES

I. Introduction

Problem Statement

The majority of research in electromigration investigates the formation of voids and open circuit failures. This is unfortunate since tests have shown that intra-level and inter-level short circuit failures due to whiskers are just as likely to cause device failure (1,2). Whiskers therefore, are a growing threat to the reliability of integrated circuits as Very High Speed Integrated Circuits (VHSIC) increase the use of multilevel metal interconnects.

Little is known about whiskers produced by electromigration compared to whiskers produced thermally. For example, research has been conducted to determine the crystallographic orientation of thermally grown whiskers (3) but not for those resulting from electromigration. A literature search has failed to reveal any documentation showing similarity between these whiskers and the processes that generated them. The nucleation process of whisker growth and hillock formation is also unknown as their location can not be predicted for an initial observation (3:162).

The primary objective of this thesis is to analyze aluminum whiskers produced by electromigration to determine their crystallographic orientation. Additional objectives include studying the nucleation, growth, and morphology of these whiskers. The study is accomplished through both static and insitu testing with a Scanning Transmission Electron Microscope (STEM). The documentation consists of diffraction patterns, bright field, and dark field photomicrographs which are analyzed to determine the whisker's crystallographic orientation, morphology, and the structure of its nucleation site.

### Major Results

The results of this study show that the crystallographic orientation of the whiskers produced by electromigration is  $\langle 110 \rangle$  along the growth axis. This information agrees with the previously determined orientation for thermally grown whiskers (3) thus providing the first evidence of their similarity.

The results also reveal a number of morphological observations through SEM and STEM micrographs. These observations include the presence of internal dislocations, surface irregularities producing striations, and mass accumulation at the base of all of the whiskers.

An original proposal is presented in Chapter IV suggesting that thermal gradients establish the effective length of the suspended stripe. It is an extension of

previously published theories regarding effective lengths (discussed in Chapter II) and suspended aluminum stripes.

### Assumptions

The following assumptions are made regarding whisker growth and suspended stripe experimentation.

1. Compressive stress is assumed or "generally accepted" as stated by Dr. Blech, to be the cause of whisker growth in electromigration (3:161).

2. Increased thermal gradients along the perimeter of the etched hole accelerate the electromigration process as demonstrated in previous suspended stripe experiments (4:264, 5:487-488, 6:170-172, 7:365). The maximum gradient occurs along the perimeter as the silicon provides a heat sink for the increased temperature resulting from Joule heating (4:264).

### Scope

The scope of this thesis is limited to the fabrication, observation, and study of aluminum whiskers with the STEM. A constant dc electric current is passed through a suspended linestripe to generate the whiskers. The study of aluminum whiskers is limited to bright field and dark field images of the whisker and grain structure, spot pattern measurements from diffraction patterns, and surface features from SEM photomicrographs.

This thesis will not study activation energies or effects due to variations in temperature and stripe

configurations since these tests have been previously performed (4,5,6,7,8,9,10).

A serpentine test pattern with widths varying from 5  $\mu\text{m}$  to 12  $\mu\text{m}$  will be used to study electromigration generated whisker growth. The composition of the stripe will be limited to pure non-alloyed aluminum (Al).

### General Approach

The following approach is designed to grow a whisker by electromigration and observe both its crystal orientation and growth process with the STEM. The process is divided into three major steps consisting of sample preparation, static testing, and insitu testing.

Sample preparation consists of processing the test stripe patterns, etching a hole through the back of the silicon (Si) die to produce a suspended linestripe, and bonding to the Mark II holder or TO-5 header. Pictures of these patterns and process descriptions are provided in Chapter III, Appendix A, and Appendix B.

The second step consists of static testing with suspended linestripes. The etched samples are bonded to TO-5 headers and powered outside of the STEM. After failure occurs, the samples are removed and inserted into the STEM where the whiskers are examined using diffraction patterns and micrographs. To examine the whisker, it must grow out of the stripe in a region which is accessible to the electron beam but thin enough for diffraction to occur.

The third step consists of conducting insitu tests within a STEM to observe whisker growth and grain morphology through diffraction patterns and micrographs taken during the electromigration process. The whiskers must meet similar area requirements as described for the static tests.

#### Major Equipment Used

The major equipment used for this thesis effort includes a JEOL 100CX Scanning Transmission Electron Microscope (STEM), a JEOL 2000FX STEM, a JEOL JXA-840 Scanning Microanalyzer, an Etec Autoscan Scanning Electron Microscope (SEM), and a Cambridge Stereogram 250 MK 2 SEM. In addition, some specially designed equipment is used as described in Chapter III. This includes the Mark II holder and its associated vacuum box.

#### Sequence of Presentation

The remainder of the thesis is divided into four chapters to provide a chronological development of the test from research to results. Chapter II presents the necessary electromigration and whisker theory for this investigation, as assimilated from a literature search.

Chapter III discusses the experimental setup and testing procedures. This includes a description of the experimental equipment, sample preparation, and testing methodology.

The test results are then presented and analyzed in Chapter IV through evidence obtained from dark field and



bright field micrographs and diffraction patterns taken with the STEM and SEM.

Finally the conclusions and recommendations for future research are discussed in Chapter V.

## II. Background

While the majority of electromigration studies have centered around the formation of voids and resulting open circuits, the growth of whiskers and subsequent short circuits was shown to be equally or even more threatening to device reliability. This fact became evident when J. R. Lloyd (2) and J. Towner (1) conducted separate experiments related to short-circuit failures in multilevel metal structures. Multilevel testing is important since metal spacing requirements are usually less between levels than with adjacent stripes (1:81). The results of these experiments revealed inter-layer metal shorts to be the dominate failure mode for the case of aluminum (Al) deposited on titanium tungsten (TiW), and intra-level shorts for the case of copper doped aluminum stripes under thick glass passivation (1:81,2:209). The importance of this failure mechanism is obvious considering the present Mean-Time-to-Failure (MTF) formula for electromigration does not address short circuit failures (1:83).

To establish the proper basis for this investigation, research was conducted in the areas of electromigration, compressive stress, whiskers, and insitu testing with a TEM. This chapter summarizes the results of previous experimentation starting with a general theory of electromigration followed by a more detailed discussion of composition gradients

and temperature gradients since they are of primary interest to the current research.

Having established the theory of electromigration, the compressive stress produced during the process is examined since it is assumed to be the cause of whisker growth (3:161). A theory is presented showing the cause-and-effect relationship between compressive stress and current density.

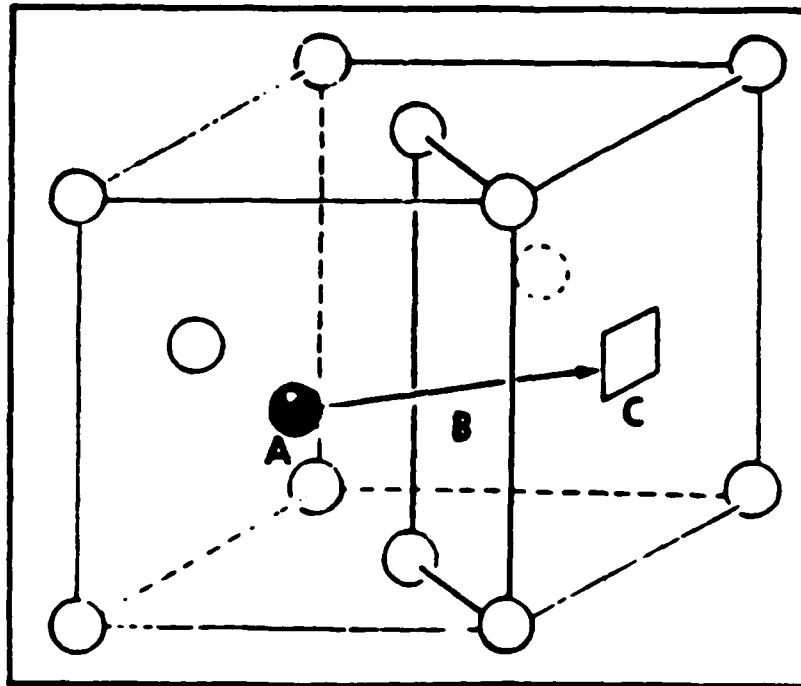
Next the results of similar research on thermally generated whiskers are examined, since they are the most closely aligned with this study.

Finally, a history of previous insitu electromigration tests using a TEM is presented. The results of these tests and their methodology establish the legitimacy of the experimental design used in this thesis.

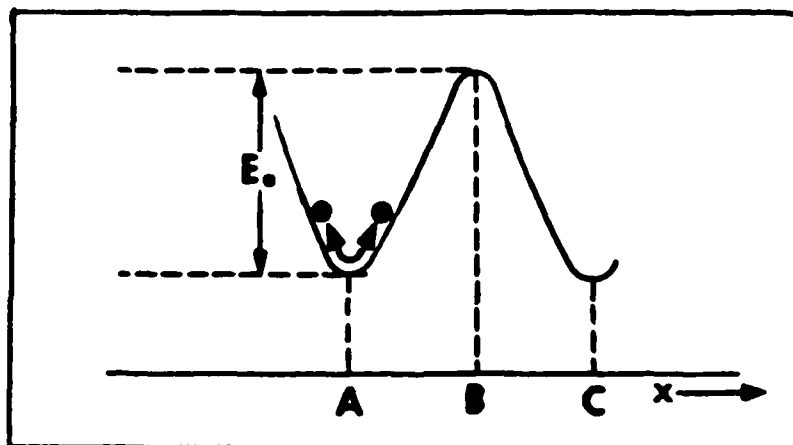
### Electromigration Theory

Huntington and others introduced the predominate theory of electromigration in 1961, describing how atoms (positive ions) are thermally excited from their lattice positions and transported toward the anode (4:263,5:485,8:338). Two models are used to describe this process. The first is the potential well model followed by the ballistic model.

Potential Well Model. The potential well model illustrates the diffusion of atoms through a metal. In pure monatomic metals, this self diffusion occurs through a vacancy mechanism as illustrated in Fig. 2.1(a) for face-centered cubic (fcc) structures (11:60,64).



(a) Vacancy Diffusion in an FCC Structure (11:64)



(b) Potential Well Model (11:39,12:147)

( $E_a$  = Activation Energy)

Fig. 2.1 Model for Vacancy Diffusion

In Fig. 2.1(a), the black atom at position A is diffusing to the vacancy denoted by the square at position C.

As the temperature increases above absolute zero, atoms acquire thermal energy and begin to vibrate about (or in the vicinity of) their lattice position (12:142). Interatomic forces from neighboring atoms hold these atoms in their lattice position. The vibration is illustrated as an ion moving up and down within its potential well as shown in Fig. 2.1(b) (11:39,12:147). If the atom acquires enough thermal energy to overcome the interatomic forces, it can move to point B where the surrounding atoms are slightly displaced. The amount of energy required to reach this point is referred to as the activation energy ( $E_a$ ). Point B is called the saddle point because there is an equal probability the atom will fall into the adjacent vacancy (C) or return to its original position (A) if no external force is applied (13:1411).

Ballistic Model. The ballistic model describes what happens to these ions in the presence of a dc current. While at the saddle point, these ions are subjected to two separate forces (8:339). The first force is an electrostatic one which is in the direction of the applied electric field ( $E$ ) (8:339). The second force ( $e$ ), of opposite direction, results from collisions with electrons flowing toward the positive anode (8:339). These forces are illustrated in Fig. 2.2 where A and C are vacancies and B is the saddle point (13:1409,1410).

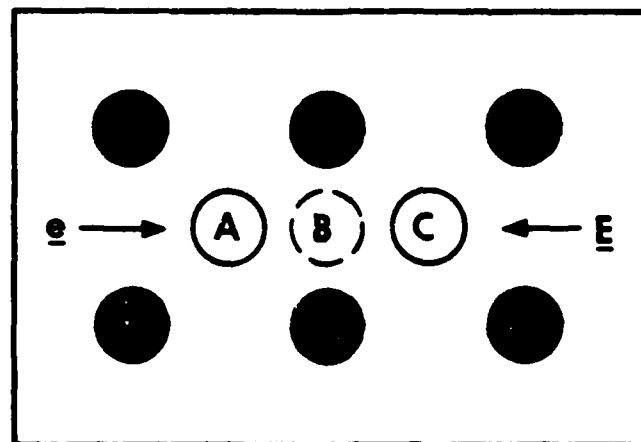


Fig. 2.2 Forces Acting on an Ion at Its Saddle Point (13)

Experimental observation in most materials has shown that the second force, referred to as an electron wind, is the more dominant force (5:485). The electron wind causes voids to form from the accumulation of vacancies at the cathode and whiskers or hillocks to form from the accumulation of ions near the anode (8:338,13:485). This observation demonstrates that mass does flow in the same direction as electrons. The accumulation of mass or voids does not occur unless there is a divergence in the flux of atoms (atomic flux) as will be mathematically shown later (13:1412).

As electrons impact the positive ions in their saddle points, the momentum transferred is  $m\bar{v}_D/t_D$ , where  $m$  is the electron mass,  $\bar{v}_D$  is the drift velocity of the electrons, and  $t_D$  is the time between collisions with positive

ions (14:5). The net momentum lost per second by all of the electrons to the positive ions is  $nm\bar{v}_D/t_D$  where  $n$  is the electron density (14:5). The average momentum transfer per second to a single ion is  $nm\bar{v}_D/Nt_D$ , where  $N$  is the density of positive ions (14:5). Substituting the electron current density  $\underline{J} = -nq\bar{v}_D$  into the average force equation gives a mathematical representation of the force due to the electron wind ( $\underline{F}_{WD}$ )

$$\underline{F}_{WD} = -m\underline{J}/[qt_DN] \quad (N) \quad (2.1)$$

where the negative sign indicates that the force is in the opposite direction of the electric field (14:5). The positive ion experiences the combination of the electrostatic force ( $\underline{F}_{ES}$ ) and the electron wind force giving (14:5)

$$\underline{F} = \underline{F}_{WD} + \underline{F}_{ES} \quad (N) \quad (2.2)$$

$\underline{F}_{WD}$  is approximately an order of magnitude greater than  $\underline{F}_{ES}$  and the effect of both forces will be taken into account shortly (13:1410).

A mathematical description (5,13) of the atomic flux  $\underline{J}_a$  is the product of the mobility ( $u$ ) of the moving atoms (positive ions) and the force ( $\underline{F}$ ) acting on them (13:1410)

$$\underline{J}_a = u\underline{F} \quad (\text{Atoms/cm}^2\text{-sec}) \quad (2.3)$$

Expanding Eq (2.3) with the Einstein relation  $u = ND/kT$  gives

$$\underline{J}_a = (ND/kT)\underline{E} \quad (\text{Atoms/cm}^2\text{-sec}) \quad (2.4)$$

where  $D$  is the diffusion coefficient of the moving positive ions,  $k$  is Boltzman's constant, and  $T$  is temperature in  $^{\circ}\text{K}$  (13:1410). The diffusion coefficient is given by

$$D = D_0 \exp(-E_a/kT) \quad (\text{cm}^2/\text{sec}) \quad (2.5)$$

where  $D_0$  is the pre-exponential diffusion constant or the diffusion constant at very high temperatures, and  $E_a$  is the activation energy (13:1410,14:94).

The force ( $\underline{F}$ ) is replaced by  $\underline{F} = qZ^*\underline{E}$ , where  $Z^*$  is the effective valence that takes into account the two opposing forces in Eq (2.2) to give (13:1410,14:5)

$$\underline{J}_a = (ND/kT)Z^*q\underline{E} \quad (\text{Atoms/cm}^2\text{-sec}) \quad (2.6)$$

A more detailed mathematical description of  $Z^*$  is given in (14:5) but it is sufficient to say that  $Z^*$  is the effective charge of the positive ion (13:1410). Substituting for the electric field  $\underline{E} = p\underline{J}$ , where  $p$  is the resistivity of the conductor and  $\underline{J}$  is the electron current density gives (13:1410)

$$\underline{J}_a = (ND/kT)Z^*qp\underline{J} \quad (\text{Atoms/cm}^2\text{-sec}) \quad (2.7)$$

Substituting Eq (2.5) for  $D$  gives

$$\underline{J}_a = (ND_0/kT)Z^*qp [\exp(-E_a/kT)]\underline{J} \quad (\text{Atoms/cm}^2\text{-sec}) \quad (2.8)$$



This equation demonstrates that the atomic flux density ( $\underline{J}_a$ ) is directly proportional to the current density ( $\underline{J}$ ) (13:1410).

The movement of atoms through a conductor does not cause failure unless a discontinuity in the flow occurs which results in depletion or accumulation (13:1411). To show this, a mass balance equation can be written for each point in a conducting strip such that

$$\partial N / \partial t = -V \operatorname{div} \underline{J}_a \quad (2.9)$$

where  $\partial N / \partial t$  gives the rate of change of positive ions and  $V$  denotes volume (4:264). The negative sign defines the direction in terms of the electron flow. By considering movement in the x-direction of the stripe, Eq (2.9) reduces to a one dimensional problem. That is,

$$\partial N / \partial t = -V \partial J_a / \partial x \quad (2.10)$$

where the scalar atomic current density ( $J_a$ ) is a function of composition ( $C$ ) and temperature ( $T$ ) such that

$J_a = J_a(C, T)$  (4:264). Substituting this function back into Eq (2.10) gives

$$\partial N / \partial t = -V [(\partial J_a / \partial C)(\partial C / \partial x) + (\partial J_a / \partial T)(\partial T / \partial x)] \quad (2.11)$$

This equation illustrates that a gradient in composition or temperature will result in "nonvanishing mass divergence" resulting in accumulation or depletion within a given region (4:264).

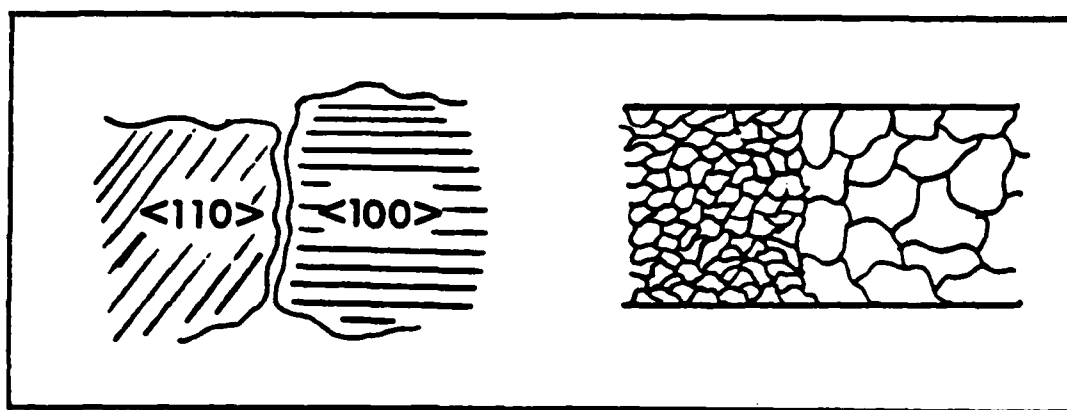
It is interesting to note another way of viewing this relationship from Eq (2.3) where  $\underline{J}_a$  changes with mobility (13:1411). Mobility, given by

$$u = (ND_0/kT)\exp(-E_a/kT) \quad (\text{atoms/N-cm}^2\text{-s}) \quad (2.12)$$

is a function of temperature and grain structure. It increases with increasing temperature and decreasing activation energy (13:1411). The latter of which is dependent upon the grain structure of the conductor (15:584).

Composition Gradients. To show how composition gradients occur, it is necessary to look first at grain structure and its effect on accumulation and depletion. An equation is needed to show how composition gradients occur.

A grain is a group of bound atoms in a lattice structure that exhibits a particular crystallographic orientation (16:5). Grain boundaries occur between grains of different orientations or sizes as illustrated in Fig. 2.3(a) and (b) respectively (13:1415). These grain boundaries may form triple points at the intersection of three grains as shown in Fig. 2.4 (17:158).



(a) Difference in Orientation      (b) Different grain sizes

Fig. 2.3 Grain Boundary Representations

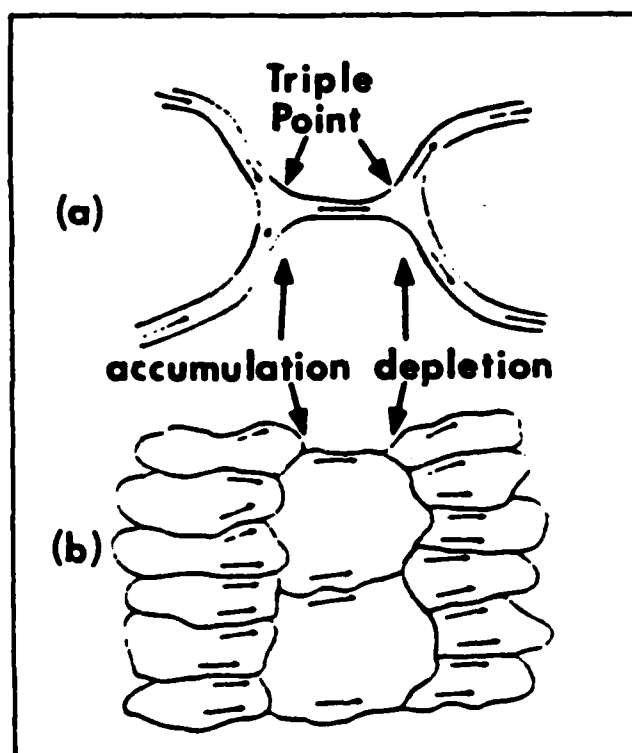


Fig. 2.4 Depletion/Accumulation at Triple Points (17:158)

Accumulation occurs when more ions enter a region than are allowed to leave, and depletion occurs where more ions exit a region than enter, see Fig. 2.4(a) (17:158). For small uniform grain sizes, this effect is minimal; however, for abrupt size changes, accumulation occurs at small/large grain boundaries, and depletion occurs at large/small grain boundaries, see Fig. 2.4(b) (17:158).

This change in ion composition with respect to the direction of atomic flow ( $x$ ) denotes a composition gradient ( $\partial C/\partial x$ ), as given in Eq (2.11). This only occurs where there is a nonvanishing divergence of atomic flux (17:158). Fick's second law gives this divergence over time as (18:55)

$$dC/dt = dJ_a/dx \quad (2.13)$$

which when expanded gives

$$dC/dt = d[(ND/kT)Z^*q_j]/dx \quad (2.14)$$

If the right hand side of Eq (2.14) is negative, there will be a negative flux divergence or depletion; however, if it is positive, there will be a positive flux divergence or accumulation (18:55).

Temperature Gradients. Temperature gradients ( $\partial T/\partial x$ ) also have an important effect on electromigration as shown in Eq (2.11). This is particularly important with suspended stripe testing as large gradients along the etched perimeter greatly enhance the electromigration process.

As device geometries decrease in size, current density ( $J$ ) increases and results in Joule heating (13:1410). Fortunately, the substrate provides good thermal conduction (Appendix C) to the ground plate (Fig. 2.5) allowing currents of up to  $10 \times 10^6$  A/cm<sup>2</sup> to flow without reaching temperatures greater than 200 °C (13:1412). Removal of the substrate however, results in heat conduction through the stripe and reduces the allowed current density.

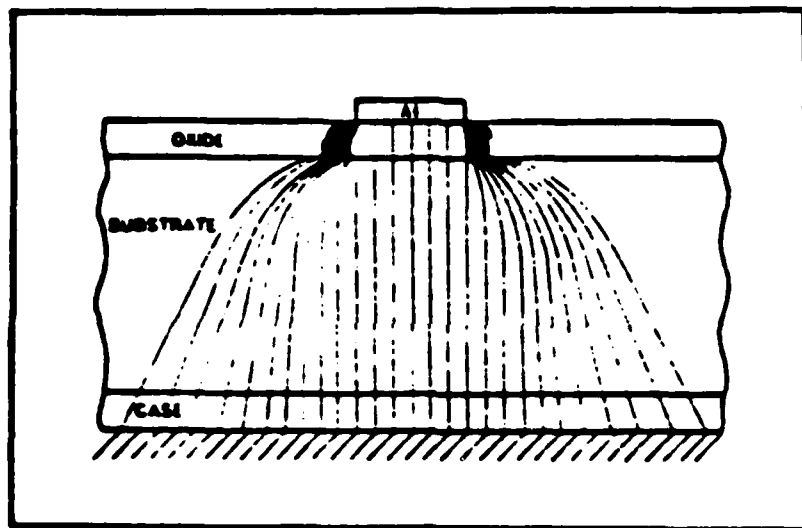


Fig. 2.5 Heat Flow From Aluminum Stripe to Ground Plate (19:26)

Dr. Blech conducted an experiment on a thin film of aluminum suspended over an etched hole in the silicon (Si) substrate, which demonstrated that voids form where electrons flow in the direction of increasing temperature, and that hillocks form where electrons flow in the direction of decreasing temperature (5:486). Since maximum heating

occurs at the center of the stripe, atoms travel in the same direction as electrons (5:487). The same experiment also shows the rate of atomic transfer to be a function of temperature since accumulation and depletion occur in the areas of greatest temperature gradients (5:487). These temperature gradients are near the cathode and anode sides of the etched perimeter away from the center of the stripe (5:487). Additional information regarding this experiment is provided in the section on previous TEM insitu experiments.

It is important to note that temperature gradients by themselves, without a dc current flow, may cause migration (13:1410). This thermal migration, called the Soret effect, occurs when there is no net current flow. Therefore, it is experimentally distinguishable from electromigration through the application of an alternating current since the current changes direction during each half of the cycle (13:1410,14:23).

### Compressive Stress

Compressive stress, which is assumed to cause whisker growth, is generated in an Al stripe through an increase in temperature resulting from Joule heating (20) or an accumulation of mass resulting from electromigration (21). The question remains as to whether or not the compressive stress is the same for both. This section presents a very cursory

discussion of thermally generated stress followed by a discussion of electromigration generated stress.

Stress Due to Temperature. Aluminum stripes on oxidized silicon wafers undergo compressive stress when heated (3,20,21). This compressive stress is primarily due to the difference in the thermal expansion coefficient of Si ( $2.5 \times 10^6 \text{ }^\circ\text{K}^{-1}$ ) and Al ( $23.5 \times 10^6 \text{ }^\circ\text{K}^{-1}$ ) (22:117,23:58). Al has the higher thermal expansion and wants to expand more than it is allowed by the Si. However, Si is the determining material due to its large mass compared to the Al and silicon dioxide (24). The formation of whiskers and hillocks may relax this compressive stress (22:124).

Stress Due to Electromigration. During the late 1970's, experiments demonstrated that stress is the dominant factor in both the minimum current density required to induce electromigration and the resulting formation of whiskers and hillocks (3). Other factors also include temperature, stripe width, and passivation layers. This section examines the experimental results which show that a stripe has a maximum level of compressive stress it can withstand before accumulation occurs. This compressive stress level is related to a critical current density which is required for electromigration to occur. It will also be shown that this critical current density is inversely related to the stripe length.

Rearranging Eq (2.8) to determine the average drift

velocity gives

$$v = J_a/N = [(D_0 q Z^* p J)/(kT)] [\exp(-E_a/kT)] \quad (\text{cm/sec}) \quad (2.15)$$

which can again be rewritten as follows (25:1203)

$$v/J = [(D_0 q Z^* p)/(kT)] [\exp(-E_a/kT)] \quad (\text{cm}^3/^\circ\text{C}) \quad (2.16)$$

Using the above equation, Dr. Blech performed experiments on an Al stripe which demonstrated a linear relationship between the average drift velocity ( $v$ ) and current density ( $J$ ) as shown in Fig. 2.6 (25:1204). He observed the rate of void growth to experimentally determine the average drift velocity (25:1204). The slope of the line is  $v/J$  and the x-intercept is the threshold current density for electromigration (25:1204).

This threshold current  $J_C$  was found to depend on stripe length, temperature, thickness, width, grain size, and passivation layers (25:1204-1205). Experimental results revealed that the threshold current density was inversely proportional to the stripe length such that the product of critical current density and stripe length ( $J_C L$ ) was approximately a constant for stripe lengths spanning the range of 30 to 150  $\mu\text{m}$  (25:1204). From this study it is easily seen that reducing the length of the stripe increases the current density it can withstand before electromigration occurs (25:1204).

Experimental results confirmed that temperature has an effect since a decrease in temperature produced a decrease



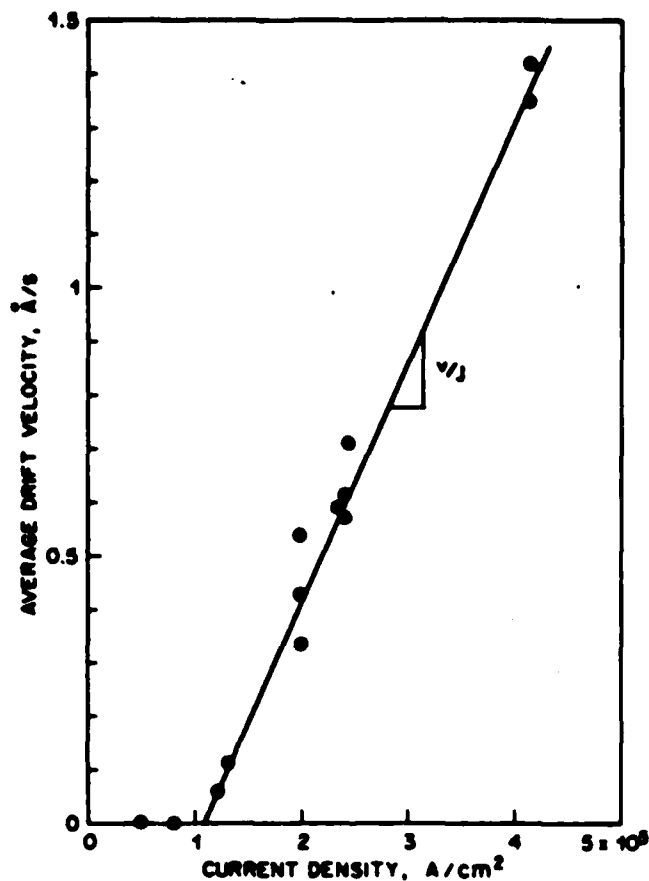


Fig. 2.6 Average Drift Velocity vs Current Density (25)

in the atomic drift velocity and an increase in the  $J_{CL}$  product (25:1204).

The width of the stripe is also an important factor dependent upon grain size. Blech notes that the drift velocity increased as the width was decreased until the width became less than  $3 \mu\text{m}$ . For annealed stripes with a width less than  $3 \mu\text{m}$ , voids and hillocks occurred along the stripe (more abundantly for annealed stripes) (25:1205). This

phenomenon is explained by Kinsborn as he experimentally demonstrated an increase in lifetime as the stripe width approaches the actual grain size (10). The reason for this is shown in Fig. 2.7 (10:969).

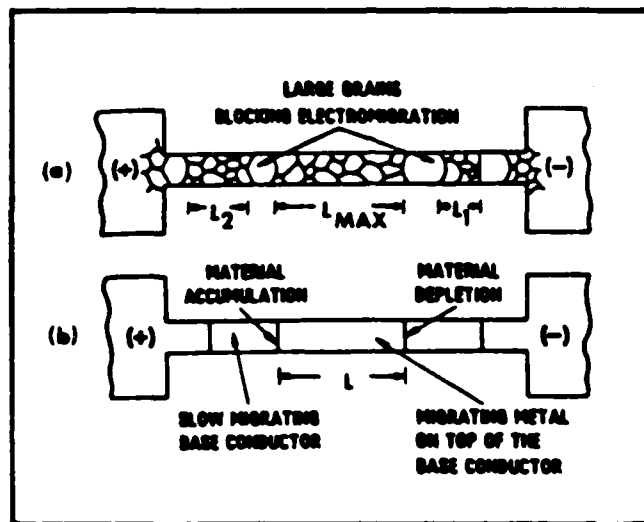


Fig. 2.7 Effective Length Reduced by Narrow Stripes (10)

At the points in which the linestripe consists of a single grain, grain boundary diffusion is stopped. As illustrated in Fig. 2.7(a), the effective length of the stripe is reduced to smaller lengths  $L_1$ ,  $L_2$ , and  $L_{MAX}$ , where  $L_{MAX}$  becomes the limiting length (10:969). Since  $J_C L$  is equal to a constant and  $L$  is reduced,  $J_C$  is increased. However, once  $J_C$  is reached for all of the segments, hillocks and voids

seem to appear throughout the stripe (10).

Blech also noted that smaller grain sizes resulted in higher drift velocities and lower current density thresholds (25:1205). This is expected, as the larger the number of grain boundaries, the more paths available for ions to take.

Finally, the use of a passivating film, silicon nitride, resulted in an increase in the  $J_C L$  product and a decrease in  $v_D$  (25:1205). However, this effect did not occur if the entire stripe was not covered. This led Blech to the following conclusion

The observation that silicon nitride layers did not affect the drift velocity when the stripes were not completely enclosed in them suggested that the retardation of electromigration is related to compressive stress buildup near the anode. (25:1205)

This compressive stress is due to the build up of atoms at the anode (25:1205). As a result, a compressive force continues to build up until it reaches a point at which additional transport cannot occur without growth (25:1205).

#### Thermally Produced Whiskers

Despite the recognition that short circuit failure between two intra-layer metal stripes is just as probable as open circuits due to voids, relatively little effort has been made to understand the whisker growth process, especially in Al. Dr. Blech has performed the most detailed work with thermally grown whiskers (3). This section identifies compressive stress as the force behind whisker growth

and examines the experimental conditions under which whisker growth was observed. The nucleation sites are then discussed relative to the observations made by Blech (3). Finally, whisker orientation and morphology are presented.

Role of Compressive Stress. For thermally grown whiskers, the compressive stress is due to the recrystallization of Al and the difference in expansion between the Al and Si (3:160). Since the whisker is the result of compressive stress, it grows from its base as if it were being "squeezed" out of the Al film (3:161).

Dr. Blech observed that whiskers grew more abundantly when the Al was covered with a film of titanium nitride (TiN) and annealed at a temperature of 350 °C (3:161). A reason was not given for using TiN as opposed to SiN or other passivation materials.

Pre-annealed films did not show any whisker growth (3:161). The unannealed stripes had a grain size of approximately 0.2 - 0.4  $\mu\text{m}$  compared to the annealed stripes with a grain size of 0.5 - 1.5  $\mu\text{m}$ . This difference indicates that compressive stress resulting from recrystallization was not as prominent for pre-annealed films. Dr. Blech also noted that short anneals usually produced hillocks while long anneals produced occasional whiskers (3:161).

Nucleation Sites. Since whisker location can not be predicted, observation of the nucleation site always started after the original nucleation when recognizable growth had occurred (3:162). The whiskers appeared to grow from both

single grains and grain boundaries as illustrated in Fig. 2.8 (3:162). A question remains as to whether or not the grains were there initially or moved into that location after nucleation (24). Through dark field micrographs, Dr. Blech did determine that the crystal orientation of the whisker and the grain at its base were different (3:162).

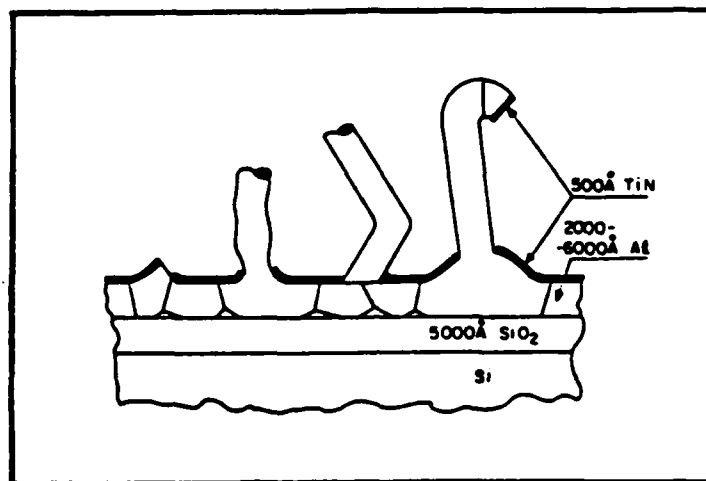


Fig. 2.8 Observed Whisker Base Morphology for Thermally Grown Whiskers (3:162)

Whisker Orientation and Morphology. Crystal orientation of four whiskers were found to be the same,  $\langle 110 \rangle$  parallel to the direction of whisker growth (3:162). Dr. Blech stated that he had previously observed, but not published, the crystal orientation of one whisker produced by electromigration to also be  $\langle 110 \rangle$  (24). This whisker had a grain

at its base with the same crystal orientation (24).

An interesting phenomena of whiskers are the striations that run from top to bottom on the stripe (24). One theory suggests that the striations appear to take the shape of the fractured TiN surrounding the base of the whisker (3:164). Another theory suggests that the striations form the outline of the surrounding grain structure at the whisker base (24).

Kinking was also observed to occur within the whiskers (3:164,167). Some of these kinks contained a boundary while others remained a single crystal (3:164).

The whisker growth rate was determined to be approximately 20 - 80 Å/s and independent of temperature (3:164).

#### Previous TEM Insitu Electromigration Experiments

The transmission electron microscope (TEM) has been used to a very limited extent in the insitu observation of electromigration. The following is a brief history of previous work including approaches, sample preparation, and results.

In 1967, I. A. Blech and E. S. Meieran observed and recorded on film, insitu electromigration within a TEM (4). The initial aluminum test stripe was 1800 Å thick on top of a 1000 Å thick oxide. To provide a path for the TEM electron beam, a hole was etched from the back of the wafer through the silicon and partially through the oxide leaving the aluminum stripe suspended over a thin layer of oxide. The sample was electrically connected to the holder with

spring clips which were electrically connected through vacuum seals to the outside. A dc current density of  $1.8 \times 10^6$  A/cm<sup>2</sup> was applied to the stripe within the TEM until failure occurred. A 60 Hz ac current was also applied in another experiment to determine if the failure was the result of thermal migration. Blech and Meieran reported that failure did not occur with the ac test.

Thermal gradients did serve to increase the rate of electromigration. Since the suspended line stripe did not have a Si substrate to provide a heat sink, the heat was conducted through the stripe to the perimeter of the hole where a Si substrate was present.

Again in 1968, Blech and Meieran performed similar tests in which they observed the growth rate of voids to determine the activation energy of electromigration in thin Al films (5). The test wafer was a 250  $\mu$ m thick, <111> oriented Si wafer on which 1000 Å of wet oxide was thermally grown. The aluminum films were deposited to a thickness of 3000 Å and etched to produce line stripes 25  $\mu$ m wide and 280  $\mu$ m long. A separate mask was then used on the backside of the wafer to pattern the region under the test stripe for Si removal using 5:3 nitric acid:hydrofluoric acid as an etchant. This stripe was also tested using a 60 Hz ac signal to verify that the migration was not due to the Soret effect. From these observations, an activation energy of  $0.7 \pm 0.2$  eV was found.

The hillocks were reported to be several times the

thickness of the stripe, and whiskers measured up to 50  $\mu\text{m}$  long and 1  $\mu\text{m}$  in diameter. Electron diffraction was used to determine that these whiskers were single crystals; however, the crystal orientation of either the hillocks or whiskers was not reported.

In 1969 it was established that doping the aluminum with 4% Cu slowed the electromigration processes (9). In 1970 S. J. Horowitz and I. A. Blech performed a similar experiment using the TEM to determine if the addition of Cu resulted in a change in activation energy. They observed the rate of void growth in doped and undoped aluminum (6). The Cu doped test stripes were 1 mil wide by 10 mils long. The JEM 7 TEM was used for the insitu observation. The test results showed a 10-100 decrease in the rate of electromigration with an activation energy of 1.1 eV for the doped aluminum vs an activation energy of .63 eV for pure aluminum.

A test team in Bratislava, Czechoslovakia conducted another insitu experiment using a TEM on Al-Cu stripes to determine the effect of preparing the stripes at different temperatures (100, 200, and 300  $^{\circ}\text{C}$ ) (7). The test wafers were 200  $\mu\text{m}$  thick Si with a thermally grown oxide of 0.1  $\mu\text{m}$ . The Al-Cu test stripes were deposited to a thickness of 0.12  $\mu\text{m}$  for each temperature. A hole measuring 0.5 by 0.5  $\text{mm}^2$  was etched through the back of the wafer using 5:2 nitric:hydrofluoric acids until it was within the final 20  $\mu\text{m}$  of Si. At that point plasma etching was performed using



freon gas ( $\text{CF}_4$ ) with 20% oxygen ( $\text{O}_2$ ) to remove the remaining  $\text{SiO}_2$ .

### Summary

A study of whiskers produced by electromigration requires knowledge of the electromigration process, compressive stress, whiskers, and testing techniques. The following is a brief summary of some of the key points presented in this chapter.

Electromigration is the movement of atoms in the direction of electron flow under a direct current. This atomic flux density is proportional to the applied current density (13:1410). Device failures due to open and short circuits only occur if a discontinuity results from temperature or composition gradients (13).

Whisker or hillock growth may relax compressive stress resulting from the accumulation of atoms (21,24,25).

A literature search has failed to produce information regarding aluminum whiskers produced by electromigration. This thesis may provide the first study directed at these whiskers.

### III. Experimental Equipment and Procedures

This chapter describes the experimental equipment and procedures used to study the formation of aluminum whiskers. A high current density is passed through a suspended aluminum linestripe to induce electromigration which results in whisker growth. The whiskers are then analyzed using scanning and transmission electron microscopy.

The sequence of presentation follows that of the thesis effort starting with a discussion of the test pattern, test equipment, and procedures used. The methods are then presented for whisker analysis and insitu observation.

#### Test Pattern

The Bridge Test Vehicle (BTV) pattern, a Bell Labs design shown in Fig. 3.1, is used for all of the experiments. It consists of four independent serpentine test stripes with varying line widths. The stripes are numbered one through four for easy referencing, and their associated line widths are specified in Table 3.1.

The BTVs are fabricated on 9 mil thick  $\langle 111 \rangle$  oriented silicon wafers. The construction of the test vehicle starts with a 5000 Å layer of silicon dioxide which is thermally grown using wet oxidation. Next, common photolithography techniques are used to define the test pattern shown in Fig. 3.1. Finally aluminum is evaporated onto the wafers and



Fig. 3.1 Bridge Test Vehicle

Table 3.1 Reference Numbers and Associated  
Line Widths for BTV Patterns

Pattern	1	2	3	4
Width ( $\mu\text{m}$ )	7.5	10	.53	.83

selectively removed to establish the test pattern. The aluminum stripes must be less than 2000 Å thick to permit the transmission and diffraction of the electron beam through the sample. Detailed fabrication procedures are provided in Appendix A.

The primary advantage of using the BTV for producing a suspended stripe is the large physical area occupied by each serpentine test stripe. This permits visual determination of where the hole should be placed on the reverse side of the chip to produce an etched region under the selected test stripe. The procedures for masking the chip and etching the silicon are provided in Appendix B.

#### Test Equipment

Before discussing experimental procedures, it is necessary to describe the configuration of the test equipment, especially the components specifically designed or modified for these tests. The test station is described first, since it houses the majority of the equipment, followed by the Mark II holder, vacuum box, and electron microscopes.

Test Station. The test station is a portable unit housing the equipment required to provide controlled electromigration testing. A block diagram of the test station is shown in Fig. 3.2 (27:C-10). The station's equipment consists of a timer, two voltage supplies, an ammeter, and two external variable resistors. The timer, shown in Fig. 3.3, is the central component of the test station and serves as the reference point for the other equipment (27:C-8, C-10). The timer provides two banana plug receptacles, labeled "EM", for connection to the BTV. These receptacles are color coded violet for positive and black for negative.

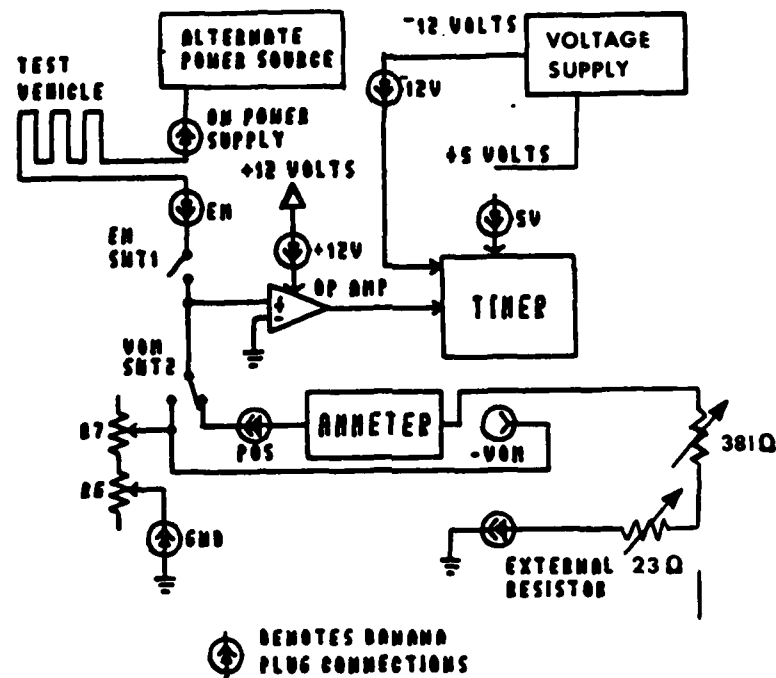


Fig. 3.2 Block Diagram of the Test Station (27:C-10)

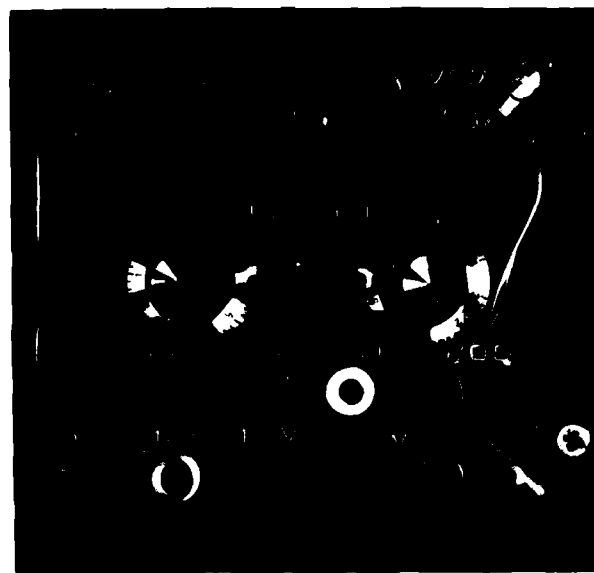


Fig. 3.3 Timer (27)

As shown in Fig. 3.2, the positive EM test port connects the test vehicle to a variable power supply. For this test station, a Hewlett Packard 6205 Dual DC Power Supply, was used to provide a variable voltage between 12 V and 50 V.

The negative EM test port connects the test vehicle to the EM switch which is used to start or stop the test and timer. When placed in the "on" position, a detecting op amp controls the internal timing circuitry sequence. The actual timing circuitry requires inputs of -12 V and +5 V to power the integrated circuits and hex displays. These voltages are provided by the Hewlett Packard 6236B Triple Output Power Supply. The banana plug receptacles on the timer are labeled accordingly for the power supply inputs with the exception of the 12 V which connects to the variable voltage supply.

The negative EM test port also connects to the VOM switch which is located at the upper right of the timer, see Fig. 3.3. In the up position, this switch permits both monitoring and controlling the current passing through the sample. The two external resistors and the variable voltage supply are used to control the current. The ammeter is a Fluke 8010A Digital Multimeter and the two external resistors are 381  $\Omega$  and 23  $\Omega$  Rex Rheostats. The larger rheostat provides coarse adjustment while the smaller provides the fine adjust.

If the sample fails or the EM switch is opened, the test and timing sequence is stopped. A reset switch is provided in the upper left side of the timer to re-initialize the timer's digital display to zero.

Additional information on the timer can be found in reference (27:Appendix C).

Mark II Holder. The Mark II holder, shown in Fig. 3.4, is used for testing within the STEM.

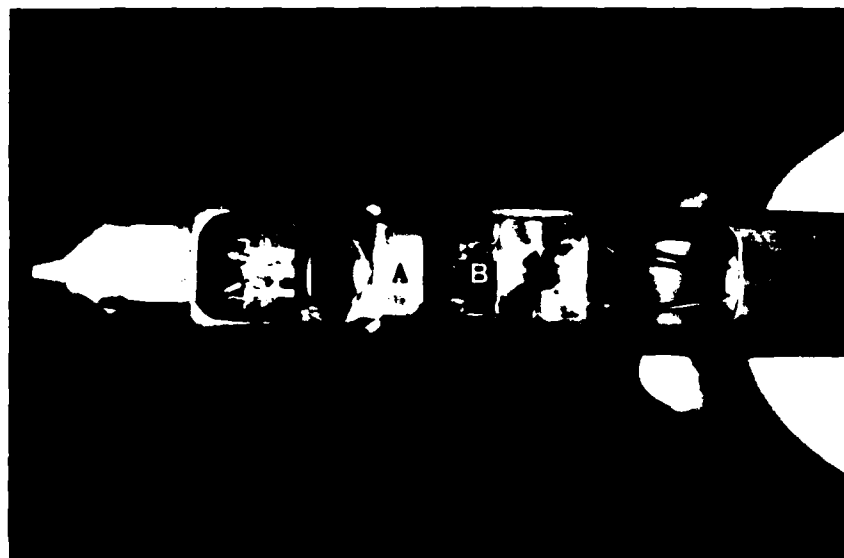


Fig. 3.4 Mark II Holder with Bonded Test Sample

The holder is a modified JEOL EM-SHH heating holder (27:III-37). The original thermocouple and furnace element were removed and replaced with an assembly (A) for mounting

and bonding a test sample (27:III-39). Electrical connections are provided through the holder's original four wires (B) to the external banana plugs (27:III-39). The banana plugs are color coded and correspond to the bonding pads as illustrated in Fig. 3.5 (27:III-47).

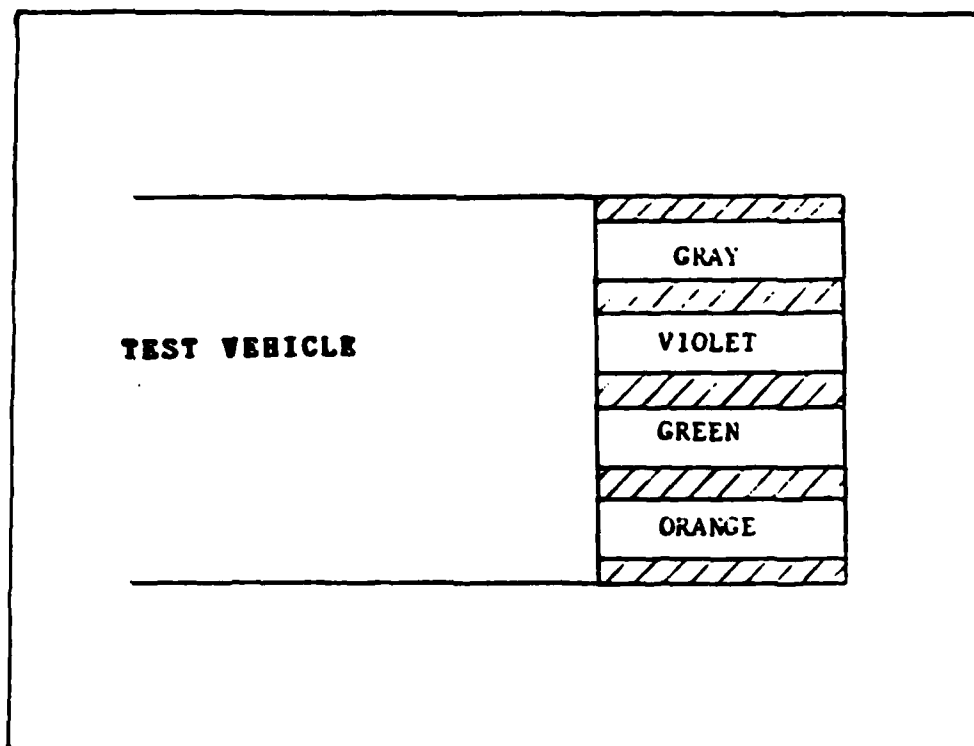


Fig. 3.5 Bonding Pads Identified by Color  
Coded Connections (27:III-47)

Vacuum Box. The vacuum box, shown in Fig. 3.6, is used to establish a vacuum environment outside of the STEM (27:III-44). Two vent ports (A) are provided such that one may be used for vacuum connection or both may be used for a



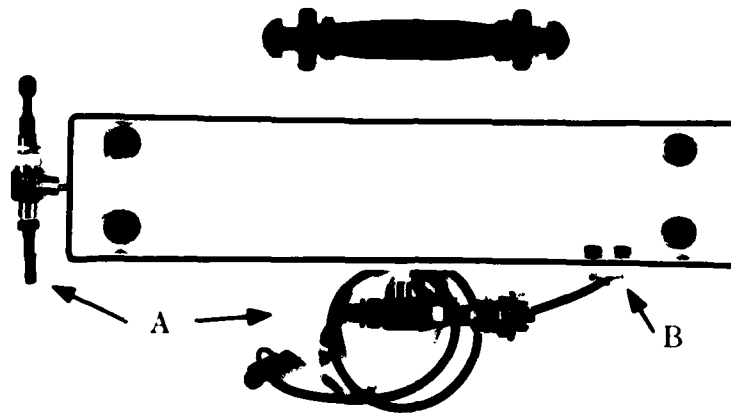


Fig. 3.6 Vacuum Box (27:III-44)

continuous nitrogen flow (27:III-44). Two sealed electrical outlets (B) are provided for external connection to the test station.

Electron Microscopes. Two STEMs, the JEOL 100CX and the JEOL 2000FX, and three SEMs; the JEOL JXA-840 Scanning Microanalyzer, the Etec Autoscan, and the Cambridge Stereogram 250 Mk 2, are used for testing and analysis. The JEOL 100CX is primarily used for insitu testing. The JEOL 2000FX is then used for whisker analysis because of its increased accelerating voltage and its ability to change magnification without rotating the image. The JEOL

Microanalyzer and the Etec Autoscan are used interchangeably for "before" pictures in static testing and the Cambridge Stereogram 250 Mk 2 is used for whisker surface examination because of its 90 degree tilt capability.

### Testing Procedures

Two types of experiments, static and insitu, are used to grow whiskers for analysis. The static testing procedures are discussed first since they form a subset of insitu testing.

Static Testing. Static testing is the most commonly used with STEMs since the sample is powered outside of the microscope and then disconnected for observation in the STEM. It is the most efficient type of test because it requires less TEM time and does not require a modified holder. The sample preparation procedures for static testing are discussed first, followed by those for the powered test.

Sample Preparation. The following procedures are used to mount and bond etched samples on TO-5 headers using conductive silver print as shown in Fig. 3.7:

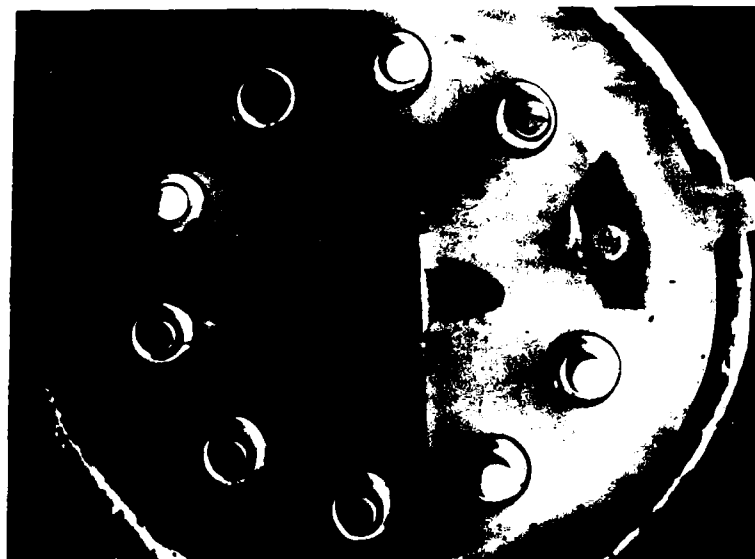


Fig. 3.7 Etched Sample Mounted and Bonded to  
a TO-5 Header

1. Distribute the silver print on the header such that it will not contact the etched region. Place the chip, pattern side up, on the print by applying light pressure to both ends. Allow five minutes for the print to dry.

The silver print is manufactured by General Cement for circuit board applications. In addition to cementing the chip to the header, it provides a heat sink to the header and a shorting mechanism for grounding unused test stripes.

2. Bond the test stripe to the posts as shown in Fig. 3.7. Avoid bonding to adjacent posts since it creates difficulty in connecting the test probes to the header leads.
3. Ground the remaining unpowered test stripes to reduce charging in the SEM. Bonding the remaining pads to other posts or shorting the patterns to ground with conductive silver print accomplishes this.
4. Ground the base of the TO-5 header with silver print to reduce charging in the SEM.
5. After bonding, trim the TO-5 header leads to within 1/4 inch of the mount.
6. Place a protective cap on top of the header to prevent accidental surface scratching or bond removal during handling and transportation.
7. Insert the trimmed mount into a modified SEM post which grounds all of the leads to prevent charging.
8. Prior to conducting the experiment, take a series of "before" pictures with the SEM to establish the condition of the stripes prior to the electromigration process. Limit these pictures to an overall picture of the entire etched region followed by a few pictures of sufficient magnification to determine the surface condition.
9. Remove the TO-5 header from the SEM post and connect the appropriate leads with probe clips to the banana plug receptacles inside the vacuum box. Note the polarity.
10. Secure the vacuum box lid with two wing nuts and apply a vacuum of 2 torr through one valve.

11. Measure the initial resistance of the test stripe and its connections. Having recorded the resistance, insert the external banana plugs into the timer's EM receptacles according to polarity.

12. Before turning on the EM switch for the powered test, make the following checks and adjustments:

- a. First, use the voltmeter to ensure all external voltages to the timer are +5V, +12V, and -12V
- b. Next, place both variable resistors into their maximum resistance position
- c. Finally, push the reset button and confirm that the six digit display reads zero.

Powered Test. The following procedures are used to start and conduct static testing.

1. Place the EM and VOM switches in the "on" position. The ammeter should register a current and a green LED in the timer should turn on and off every six seconds.

2. Adjust the current to the desired level with the external resistors and external voltage supply. This voltage may be increased to 50V without damaging the timer since the op amp driver has built-in overdrive protection. Once the current has stabilized, the test station can be left running and unattended.

The electromigration process can be monitored to a limited extent by observing changes in the current. As void formation increases, the resistance of the stripe increases

and the current decreases. However, it is impossible to predict the exact time of failure.

The process can be interrupted as follows for a visual inspection in the SEM.

1. Slowly decrease the current to minimize the sudden change to the stripe. Turn the EM switch off.
2. Record the time in the event the power is removed from the timer.
3. Carefully remove the sample from the vacuum box and transport it to the SEM.
4. Resume the test by following the same procedure described earlier for starting.

Once the test is completed, the sample is removed from the header and mounted to a copper bulk holder as shown in Fig. 3.8 for TEM analysis. Silver print is used to mount the chip and short all the test stripes. The TEM analysis procedures are discussed later following the insitu testing.

Insitu Testing. Insitu testing allows the analysis to be performed as the electromigration process occurs. Test samples are bonded to the Mark II holder and inserted into the STEM. The holder's external banana plugs are connected to the test station in the same manner as the static test. This permits the application of current to the stripe while simultaneously observing its effect in the STEM.

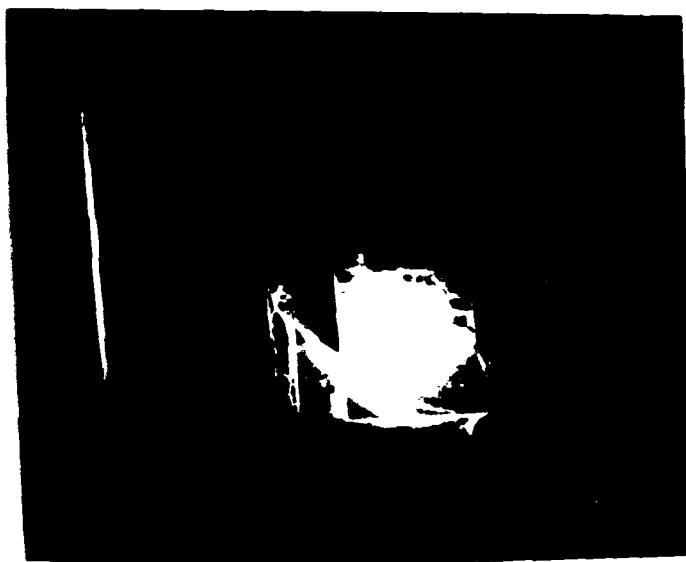


Fig. 3.8 BTV Mounted to a Copper Bulk Holder  
After Static Testing

The sample preparation is discussed first followed by a brief description of the powered test which is similar to static testing. The insitu testing methodology is discussed later since it requires knowledge of the analysis procedures.

Sample Preparation. For insitu testing, use the following procedures to mount the sample in the Mark II holder with silver print as shown in Fig. 3.9.



Fig. 3.9 Sample Bonded to the Mark II Holder

1. Place the chip in the holder with the etched region over the hole in the mounting assembly. It is advantageous, for bonding purposes, to orient the sample such that the test pads are on the opposite side of the hole from the holder's bonding pads.

2. Ground the unpowered stripes with silver print to the mount assembly to reduce charging from the STEM electron beam. Use an ohmmeter to ensure electrical continuity. This is critical since the stripes are often damaged during bonding and transport.

3. Insert the Mark II holder into the STEM and connect all four banana plugs to ground for the "before test" pictures. These pictures consist of low magnification Bright



Field (BF) micrographs depicting the stripe condition, high magnification BF micrographs showing grain size, and diffraction patterns.

4. Disconnect the two test lines from ground and insert them into the timer's EM plugs according to polarity. The unused lines remain grounded to reduce charging.

5. At this point, perform the same pre-test checks and adjustments as described for the static testing.

Powered Test. This part of the process is the same as the static with the exception of the capability to directly observe the electromigration as it occurs. The analysis procedures described later are used as necessary throughout the test.

After a test is stopped due to failure or termination, the leads are removed from the EM jacks and reconnected to ground for a final analysis.

#### Whisker Analysis Procedures

The analysis portion of this study requires the application of an electron microscope, primarily a STEM. The following methodology is used to examine whiskers with respect to their orientation, morphology, and site of nucleation.

Inspection. The initial examination of the whisker is performed with the STEM to avoid possible contamination from the SEM. Bright field microscopy is first used to examine the test stripes to determine if any whiskers were produced.

The stripes are also examined for the presence of electromigration, which implies voiding near the cathode and accumulation near the anode.

During the inspection, a decision is made regarding the best approach in analyzing a whisker. If the whisker protrudes away from the aluminum stripe, over a thin layer of oxide, it can be examined as is. If the whisker lies over the aluminum stripe, replication is necessary for diffraction analysis. Before replicating, SEM micrographs are taken of the whisker for structural analysis.

Bright Field Micrographs. A series of bright field (BF) micrographs are taken regardless of the whisker's location. These BF micrographs provide a transparent picture of the whisker detailing its internal characteristics.

Diffraction Patterns. The next step in the analysis is determining the whisker's crystallographic orientation through diffraction patterns. The sample is placed in the STEM such that the electron beam passes through the whisker. The STEM is then placed in a diffraction mode which produces a diffraction pattern on the viewing screen from Bragg reflection. Since the whiskers are single crystals, the diffraction pattern is a spot pattern. Next, the whisker is aligned and tilted until a spot pattern is produced with one or more spots parallel to the whisker.

Dark Field Micrographs. A second test is conducted to ensure that the whisker produces the spot lying parallel to the whisker. The spot is electronically positioned in the

center of the viewing screen along the optic axis. The STEM is then placed in a dark field mode wherein the spot's contributors appear bright against an otherwise darkened background. If the whisker produces the spot, the whisker appears bright.

The calculations and mapping procedures for the diffraction patterns are presented in Chapter IV.

SEM Micrographs. The SEM is used to study the surface features of the whisker and its originating test stripe. The main objectives include showing the whisker's striations, cross-section, and base. To enhance the image, a thin layer of gold (approximately 100 Å) is sputtered onto the surface of the chip.

#### Insitu Observation Techniques

During the insitu test, it is difficult to observe the whisker's nucleation since its nucleation site cannot be predicted or controlled. The best approach is to pick the longest test stripe over the etched region and closely monitor its anode side during the test. The best detail is obtained using the STEM in the bright field mode. Micrographs are taken periodically to record the electromigration process. The ammeter is also monitored for any significant decreases in current which signals an impending failure. The test is terminated before failure to reduce damage to the test stripe.

### Summary

The Bridge Test Vehicle (BTV) is used for all of the tests because of the advantage offered in etching holes beneath any of its four serpentine test stripes. Each stripe occupies an area large enough to permit visual application of the wax mask under the desired test stripe.

The test equipment is set up to provide a controlled current and a measure of the time to failure. The unique pieces of test equipment are the timer, Mark II holder, and the vacuum box.

While the test procedures are different for static and insitu tests, the analysis techniques are the same. These techniques describe how information regarding the whisker's orientation and physical characteristics are acquired.

Having completed the test and analysis, the results of the study are presented in the next chapter.

#### IV. Results and Discussion

This chapter presents and analyzes the results obtained from the experiments described in Chapter III. The suspended test stripes are discussed first to establish that electromigration did occur. Next the whiskers are examined in relation to their crystallographic orientation and morphology.

##### Electromigration

A study of whiskers produced by electromigration requires an analysis of the test stripes to determine if electromigration was indeed the cause. This section presents test results to establish that electromigration did occur.

Fig. 4.1 is an SEM micrograph of an etched sample after failure. The polarity of the stripes are shown at the top and bottom of the picture. Accumulation does occur on the positive side of stripes (B, C, and D). Although it is not evident in the micrograph, voiding also occurred on the negative side of stripes B and D. The open circuit failure from voiding occurred at x on stripe C. These results confirm that electromigration did occur since accumulation occurred near the positive edge while voiding occurred near the negative edge of the suspended stripes.

For these tests, relatively low current densities of approximately  $0.45 \times 10^6$  A/cm<sup>2</sup> were used compared to typical values of  $3 \times 10^6$  A/cm<sup>2</sup> for unetched testing. The lower

current density has been attributed to the accelerated electromigration resulting from the increased thermal gradients along the perimeter of the etched region (4:265). It is proposed that these thermal gradients may also establish the effective length ( $L_{MAX}$ ) in relation to the  $J_C L$  product. Observations of suspended test stripes with varying lengths under identical current densities support this theory. As shown in Fig. 4.1, the failure occurs in the longest stripe (C). Evidence of electromigration decreases with length (B and D) until it is no longer evident in shorter stripes (A, E, and F).

According to the  $J_C L$  product discussed in Chapter II, the critical current density required to induce electromigration decreases as the length of the test stripe increases. The concept of thermal gradients establishing the  $J_C L$  product in suspended linestripes appears to be original and recommendations for additional testing with varying suspended stripe lengths are provided in Chapter V. The thermal model for suspended stripes is presented in Appendix C.

Separate tests for thermal migration using an ac current source were also conducted and are presented in Appendix D. These tests appear to be inconclusive, however.

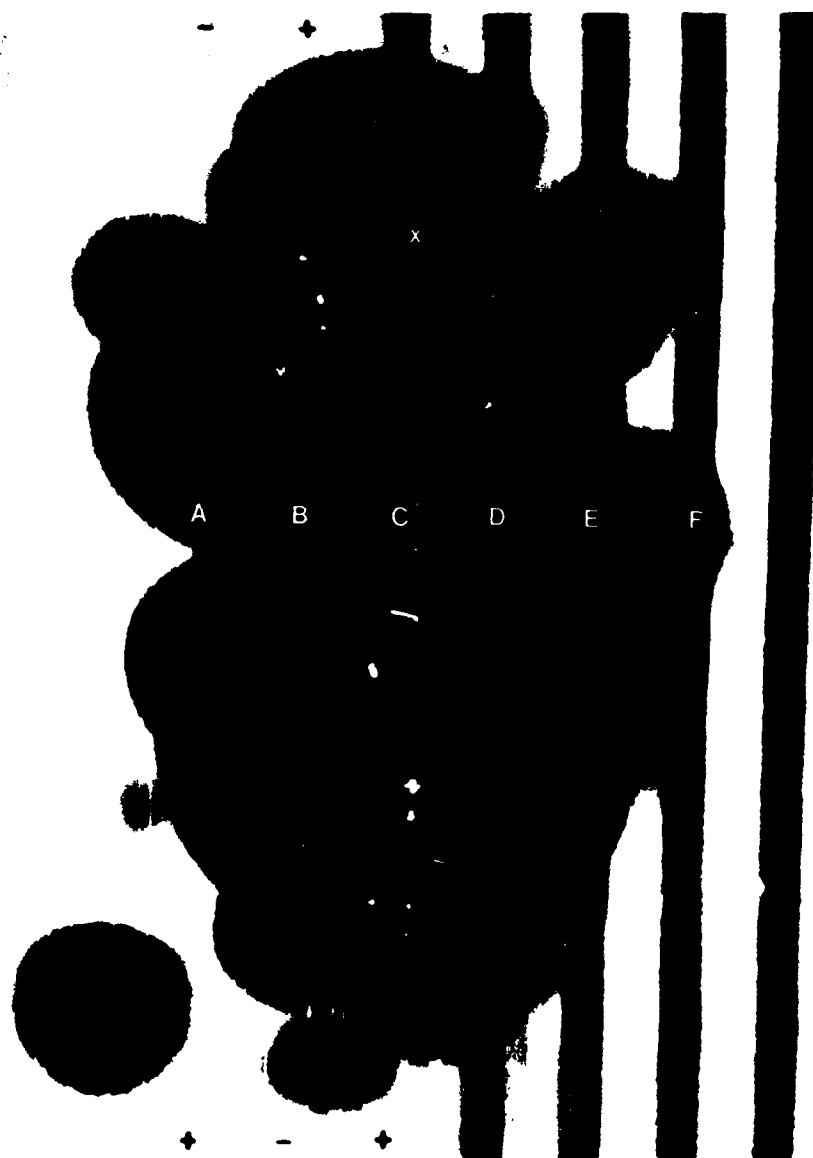


Fig. 4.1 Observation of Increased Electromigration in  
Longer Stripes (Magnification = 6K)

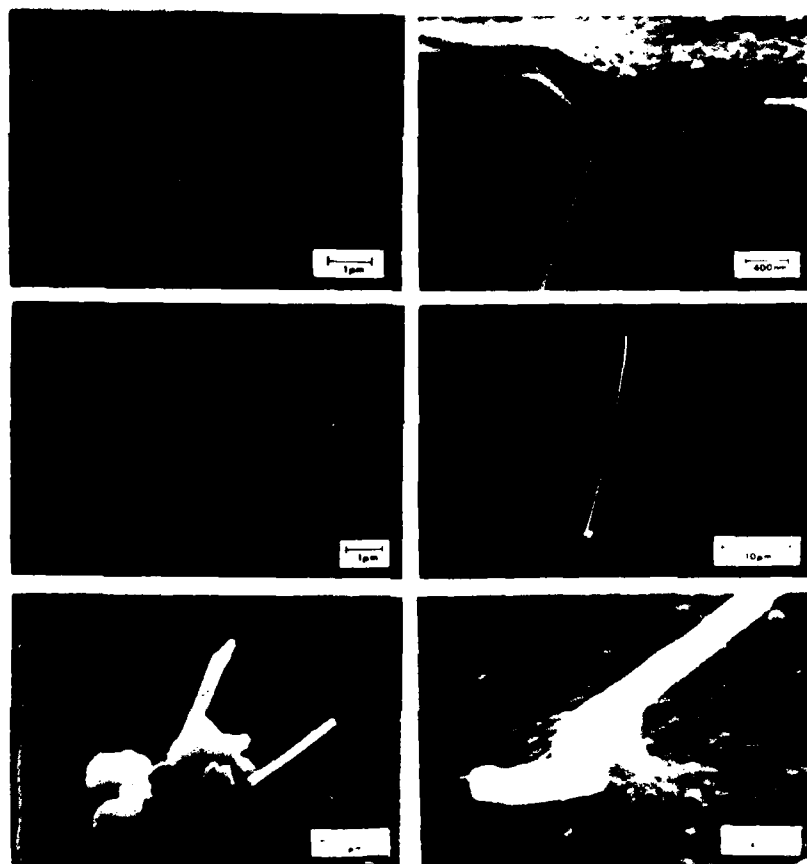
### Results of Whisker Analysis

A number of whiskers were successfully grown and analyzed with the electron microscopes. Table 4.1 presents a summary of the test conditions and results for 12 whiskers shown in Fig. 4.2 and 4.3.

Table 4.1 Crystallographic Orientation and Test Condition Information for Each Whisker

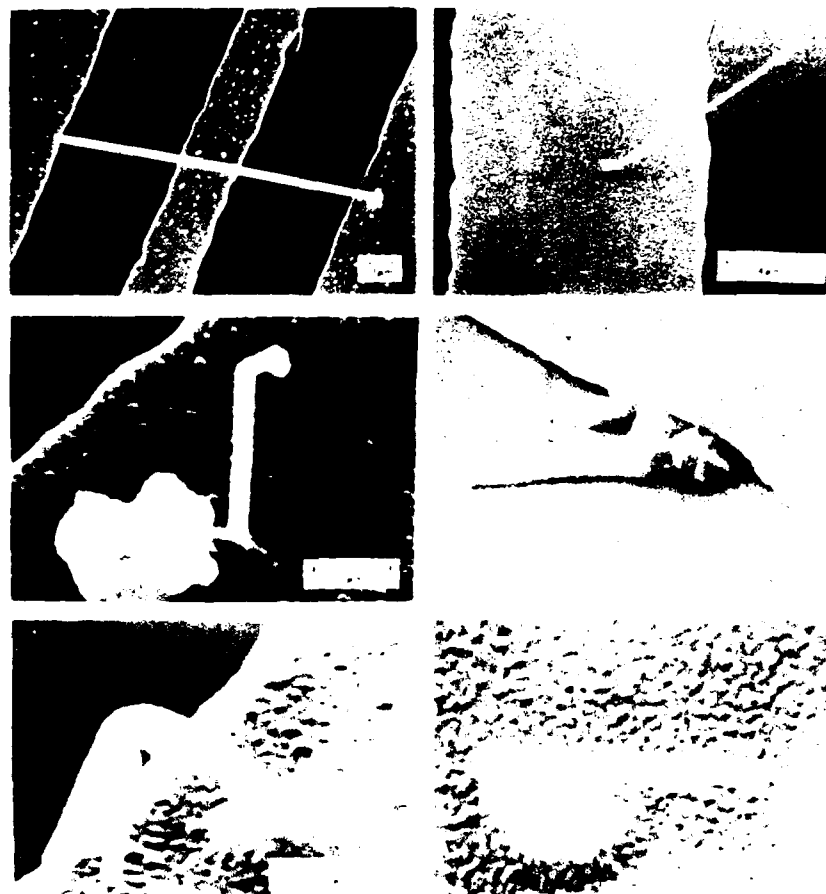
Category	Whisker #											
	1	2	3	4	5	6	7	8	9	10	11	12
Orientation< >	110	110	110	110	-	-	-	110	-	-	-	-
Current Density MA/cm <sup>2</sup>	.47	.47	.56	.56	.48	.48	.48	.48	.48	.48	.48	.48
Length of Test Stripe ( $\mu$ m)	276	198	236	236	243	267	266	300	300	300	266	350
Width of Test Stripe ( $\mu$ m)	12	12	10	10	12	12	12	12	12	12	12	12
Test Time (min)	240	240	376	376	58	58	58	58	58	58	58	58
Test Type Static-S Insitu-I	S	S	S	S	I	I	I	I	I	I	I	I





1	2
3	4
5	6

Fig. 4.2 SEM Micrographs of Whiskers #1 - #6



7	8
9	10
11	12

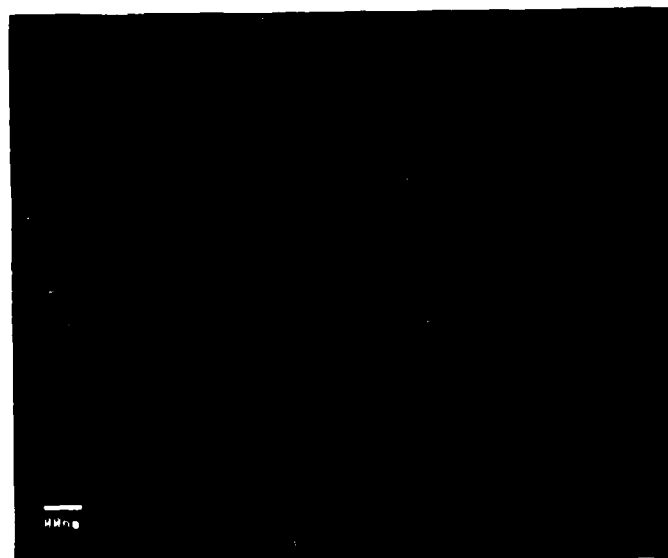
Fig. 4.3 SEM Micrographs of Whiskers #7 - #12

The whiskers are arbitrarily numbered for easy reference. This section presents the results of this analysis starting with the crystallographic orientation.

Crystallographic Orientation. Five whiskers were examined and determined to have a  $\langle 110 \rangle$  orientation along the growth axis. This agrees with the findings of Dr. Blech for thermally grown whiskers. The remaining seven whiskers were not accessible for diffraction patterns.

The crystallographic orientation of the whiskers was determined using the procedures described in Chapter III. For example the bright field micrograph was obtained first as shown in Fig. 4.4a for Whisker #1. Next a diffraction spot pattern was obtained such that two of the spots were parallel with the whisker axis. A dark field image of the (220) spot confirmed that it was produced by the whisker which appears bright in Fig. 4.4b. Although part of the whisker appears darker in Fig. 4.4b, the brightest section was observed throughout the whisker by adjusting the condenser lens. The condenser lens focuses the electron beam onto the whisker which indicates that the whisker was tilted such that only a portion of it could be focused into the back focal plane of the TEM. The indexed spot pattern of whisker #1 is shown in Fig. 4.5 with a key which illustrates the spot location and corresponding angles.

The spot patterns of the four remaining whiskers are shown in Fig. 4.6 through Fig. 4.9 followed by a discussion of the analysis technique used to index the spot patterns.

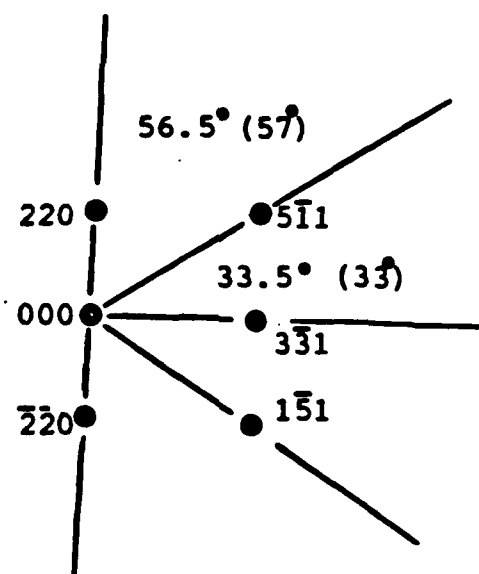
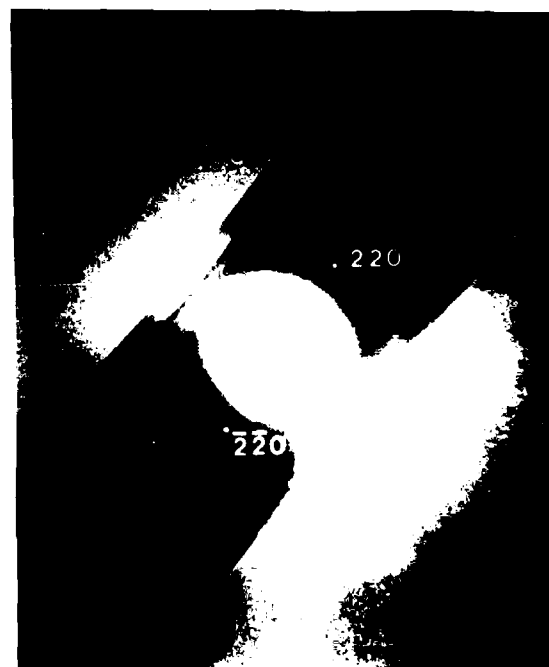


(a) Bright Field Micrograph of Whisker #1



(b) Dark Field Micrograph of Whisker #1 With the (220)  
Spot Placed on the Optic Axis

Fig. 4.4 Bright Field and Dark Field Micrographs of  
Whisker #1 (Magnification = 25K)



5.5° OFF WHISKER

Fig. 4.5 Double Exposure of Spot Pattern and Bright Field  
Micrograph for Whisker #1 (Magnification = 41K)

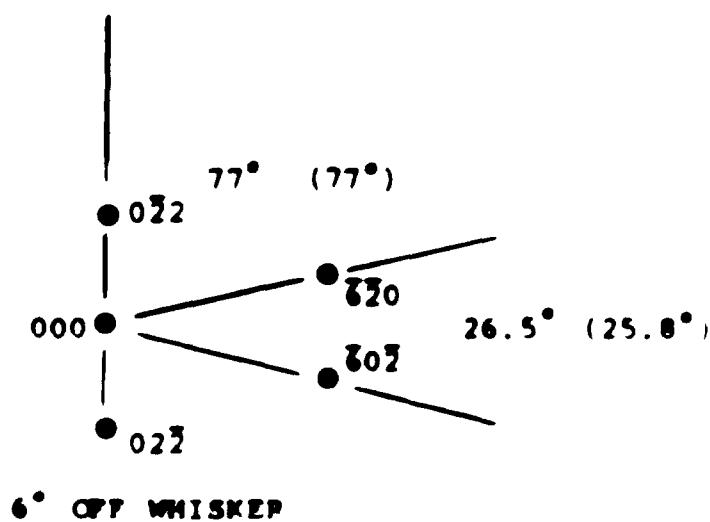
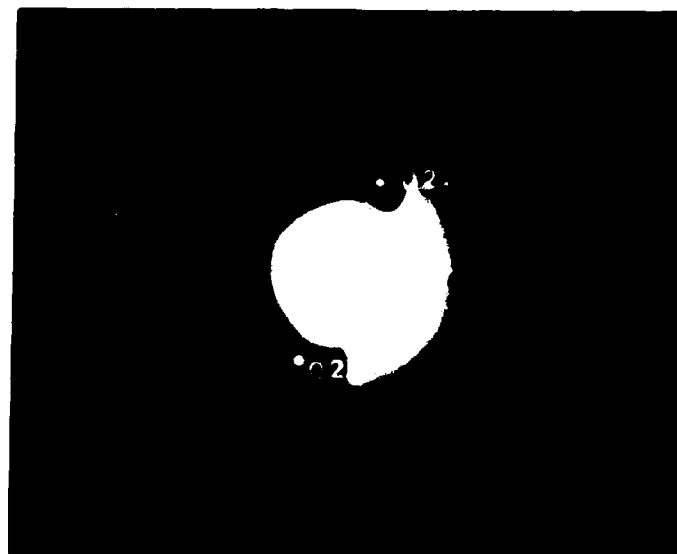


Fig. 4.6 Double Exposure of Spot Pattern and Bright Field Micrograph for Whisker 8.

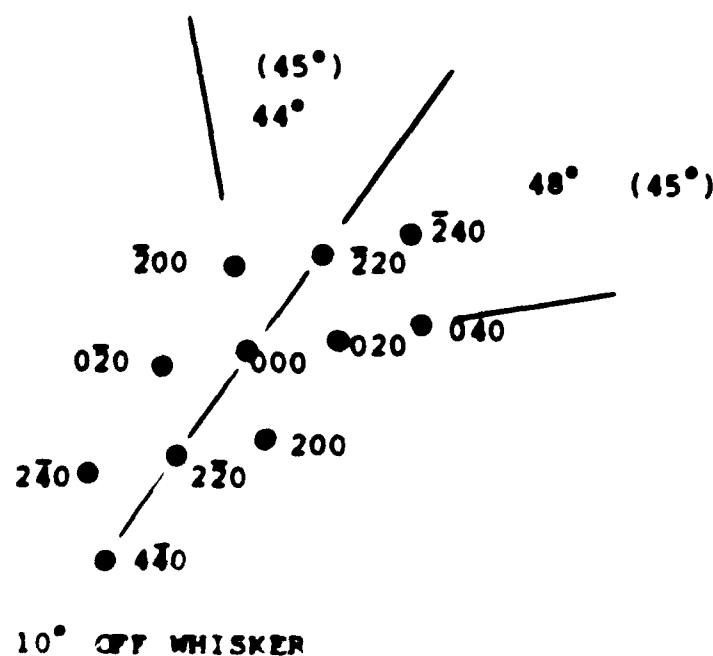
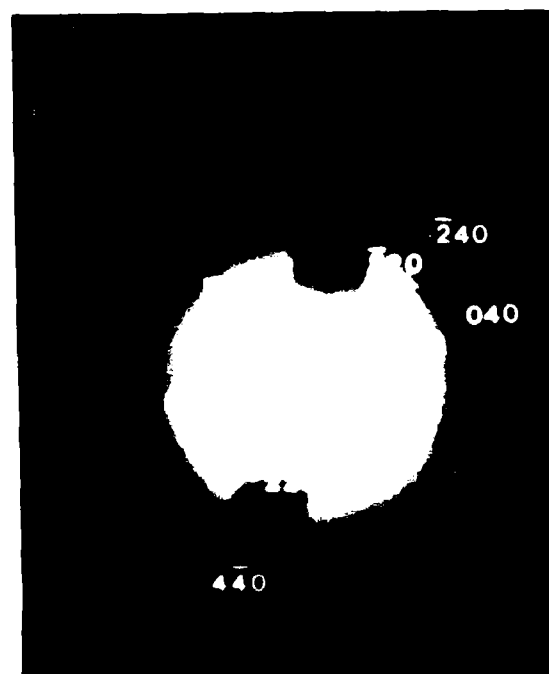


Fig. 4.7 Double Exposure of Spot Pattern and Bright Field  
Micrograph for Whisker #1

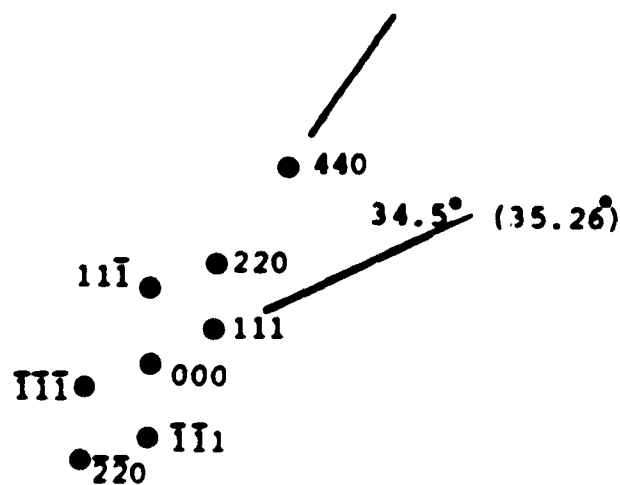
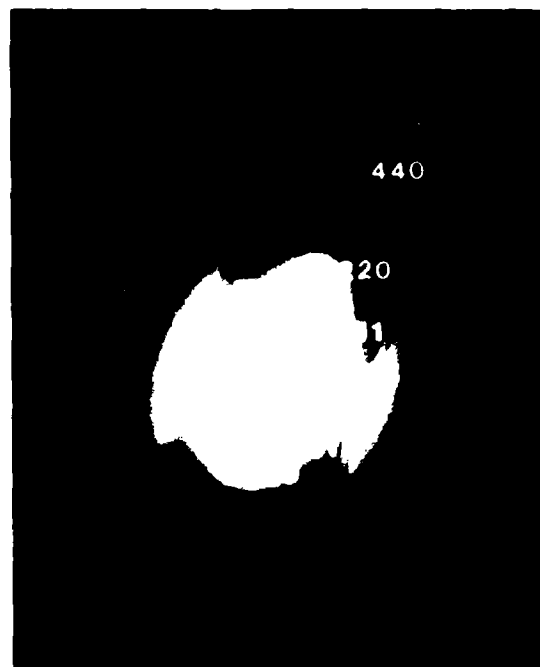


Fig. 4.8 Double Exposure of Spot Pattern and Bright Field  
Micrograph for Whisker #4



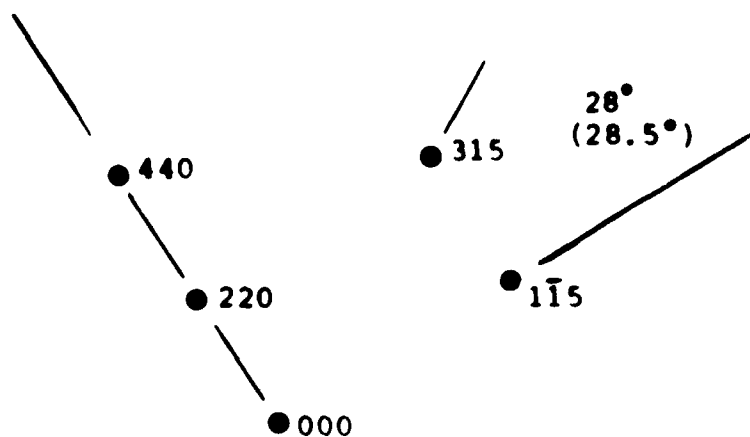
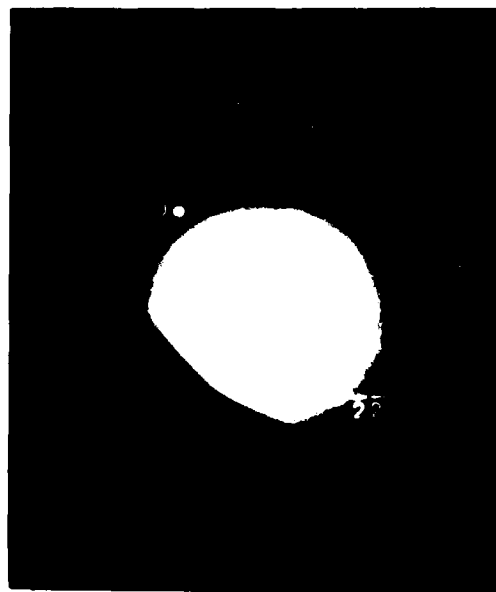


Fig. 4.9 Double Exposure of Spot Pattern and Bright Field  
Micrograph for Whisker #8

Spot Pattern Analysis. The crystallographic orientation of the whisker is found using the spot pattern and the originating stripe's ring pattern. A calibration of the Al ring pattern is performed first with a standard Al sample.

Calibration of Al Diffraction Rings. The calibration of the Al diffraction rings was accomplished using a standard Al sample. The resulting ring pattern is shown in Fig. 4.10.

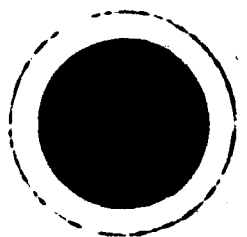


Fig. 4.10 Diffraction Pattern Produced By Aluminum Standard

The camera constant of the STEM ( $\lambda L$ ) was measured according to

$$rd = \lambda L \quad (\text{\AA cm}) \quad (4.1)$$

where

- $r$  = radius of the spot or ring (cm)
- $d$  = interatomic spacing ( $\text{\AA}$ )
- $\lambda$  = wavelength of the electron ( $\text{\AA}$ )
- $L$  = the distance from the object to the image plane (cm)
- $\lambda L$  = the camera constant ( $\text{\AA cm}$ )

The  $d$  values are provided with the standard. The error percentage for the first five rings must be less than 1% (28). The resulting camera constant for the JEOL 100CX from Fig. 4.10 is 2.563  $\text{\AA cm}$ .

Fig. 4.11 shows the ring pattern of a standard Al thin film on the left and a test stripe on the right. The diffraction pattern on the left was produced with a 100 KV accelerating voltage while that on the right was produced with a 200 KV accelerating voltage. Unfortunately the camera constant changes with focusing and accelerating voltage. This problem is avoided using the ratio test.

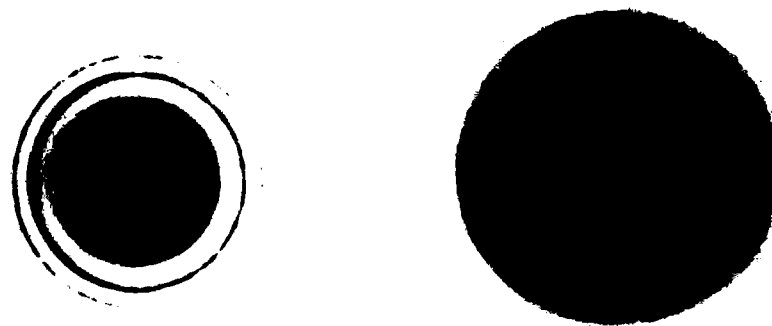


Fig. 4.11 Diffraction Patterns of the Al Standard at 100 KV  
and Test Stripe at 200 KV

Ratio Test. The ratio test is derived from Eq  
(4.1) as follows

$$r_1 d_1 = \lambda L = r_2 d_2 \quad (\text{Acm}) \quad (4.2)$$

$$r_1 d_1 = r_2 d_2 \quad (\text{Acm}) \quad (4.3)$$

$$r = D/2 \quad (\text{cm}) \quad (4.4)$$

$$D_1 d_1 = D_2 d_2 \quad (\text{Acm}) \quad (4.5)$$

$$d_1/d_2 = D_2/D_1 \quad (4.6)$$

where D is the diameter of a ring, the postscript 1 refers to the innermost {111} ring, and the postscript 2 refers to any other ring.

The ratios of the measured ring diameters are compared to the standard ratios of the interatomic plane spacings shown in Table 4.2.

Table 4.2 Interatomic Distances and Ratios (28)

( $d_x/d_1 = x \text{ distance}/\{111\} \text{ distance}$ )

hkl	d	dx/d1
111	d <sub>1</sub>	1.0
200	d <sub>2</sub>	0.8476
220	d <sub>3</sub>	0.5992
311	d <sub>4</sub>	0.5113
222	d <sub>5</sub>	0.4895
400	d <sub>6</sub>	0.4240
331	d <sub>7</sub>	0.3890
420	d <sub>8</sub>	0.3791
422	d <sub>9</sub>	0.3461

If the ratios match, the material is aluminum. The ratios also establish the (hkl) indices assigned to each ring on the diffraction pattern and its associated radius.

Mapping the Spot Pattern. The spot pattern is analyzed using the radius measurements of the rings. Each spot is assigned a generic (hkl) combination based on distance from the center alone. For example, the spots in Fig. 4.12(a) are assigned (hkl) indices based on their radius. The order or sign conventions of these spots are then

determined through vector addition or subtraction as shown in Fig. 4.12 (b) and (c) (29:46,47).

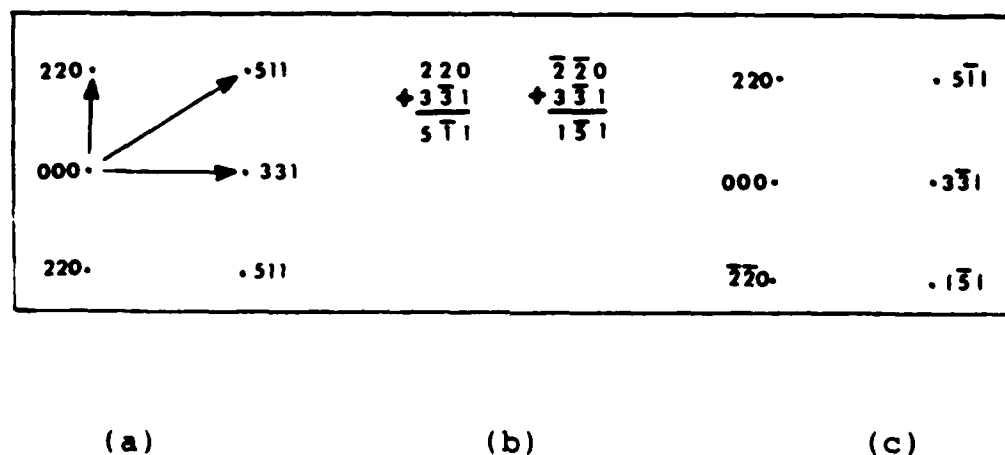


Fig. 4.12 Mapping of Spot Patterns for Whisker #1

One spot is arbitrarily assigned to establish the possible values for the other spots. The (220) spot could have just as easily been designated (202), since the {220} family are all crystallographically equivalent.

To verify the mapping solution, the angles between the (hkl) planes are calculated using

$$\cos \theta = \frac{[h_1 h_2 + k_1 k_2 + l_1 l_2]}{[(h_1^2 + k_1^2 + l_1^2)^{\frac{1}{2}} (h_2^2 + k_2^2 + l_2^2)^{\frac{1}{2}}]} \quad (4.7)$$

The calculated and measured angles must match if the pattern is mapped correctly. According to Eq (4.7) for Whisker #1, the angle between (220) and ( $5\bar{1}1$ ) should be  $57^\circ$  and the angle between ( $5\bar{1}1$ ) and ( $3\bar{3}1$ ) should be  $33^\circ$ . The measured angles are  $56.5^\circ$  and  $33.5^\circ$  respectively resulting in errors of only .88% and 1.5%.

In some instances as with Whisker #2, the spot pattern matches a predefined pattern as shown in Fig. 4.13 (29:305).

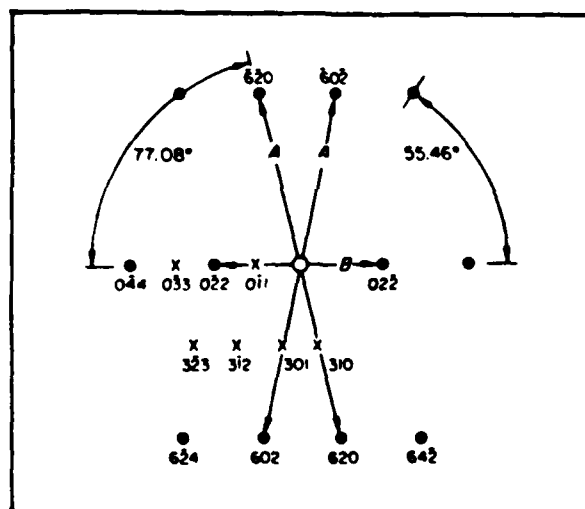


Fig. 4.13 Pre-Mapped Spot Pattern (29:305)

A comparison of the (hkl) values and angles permits easy identification.

### Determining the Orientation of the Whisker.

The spots lying parallel to the whisker's growth axis are used to determine the orientation of the whisker as illustrated in Fig. 4.14 (30:232).

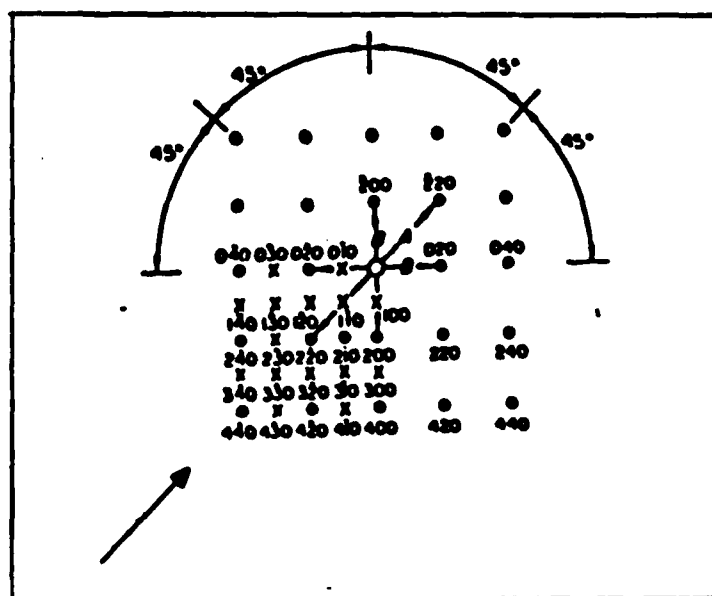


Fig. 4.14 Spot Pattern With the Whisker Axis  
Indicated by an Arrow (29:304)

The (220) spot represents all of the (220) planes. An arrow drawn from the origin perpendicular to the (220) plane establishes the [220] direction.

If the JEOL 2000FX is used, it is easy to determine which spots lie parallel to the whisker since there is virtually no rotation between bright field images and diffraction patterns. If the 100CX is used, rotation calibration charts establish the correct axis.



Orientation Results. The results of this analysis show that all of these whiskers are oriented in the  $\langle 110 \rangle$  direction. All of the mapped patterns show crystallographically equivalent directions of  $\langle 220 \rangle$  which is the same as  $\langle 110 \rangle$ . Errors up to 10 degrees are seen between the whisker's growth axis and the  $\langle 110 \rangle$  direction. This may be due to a very small rotation in the JEOL 2000FX. Problems with the microscope precluded a rotation calibration. A previous study of tin whiskers also indicated similar errors (30:232).

Morphology. The morphology of the whiskers was also examined for any information concerning their structure or nucleation. This section presents some very interesting findings.

Internal Structure. The STEM micrographs reveal internal dislocations throughout the whiskers. Whisker #2 provides an excellent example of this as shown in Fig. 4.15. The dislocations are the dark lines running perpendicular to the whisker. Dr Blech also noticed similar dislocations in the thermally grown whiskers but attributed them to the removal of the whiskers from the test film (3:162). Since these whiskers were not removed, the dislocations apparently occurred during the growth process. The type or nature of the dislocations was not determined.

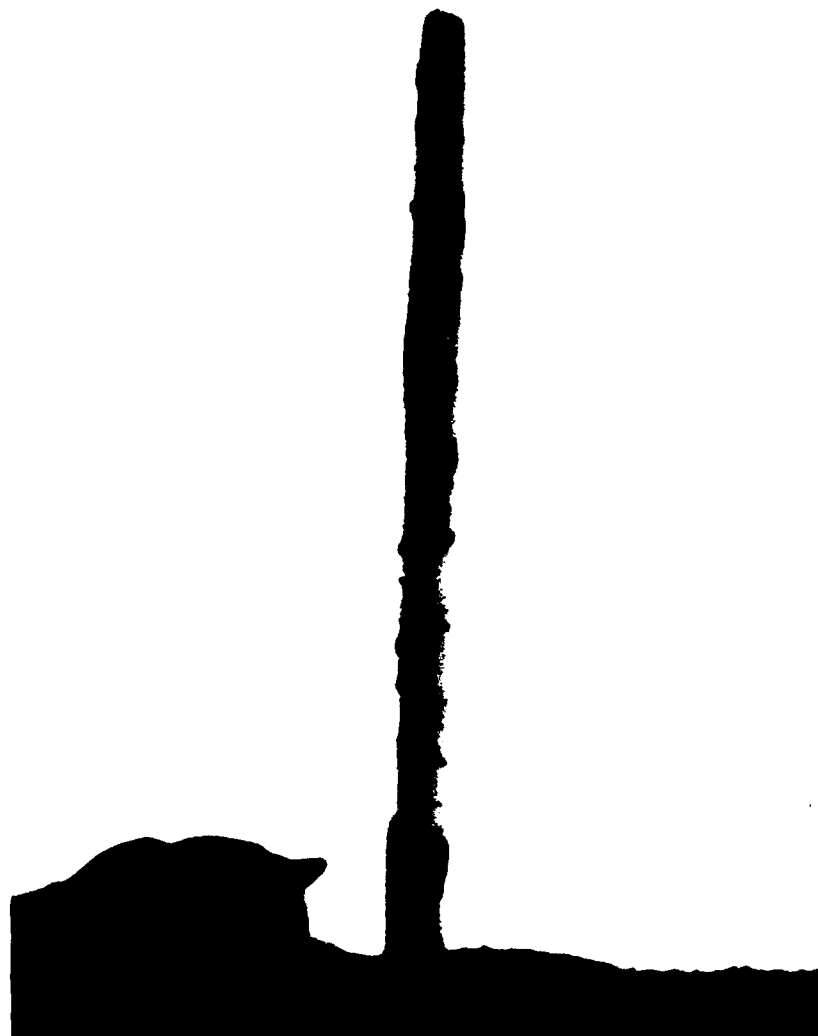


Fig. 4.15 Bright Field Micrograph of Whisker #2 Depicting  
Internal Dislocations (Magnification = 23K)

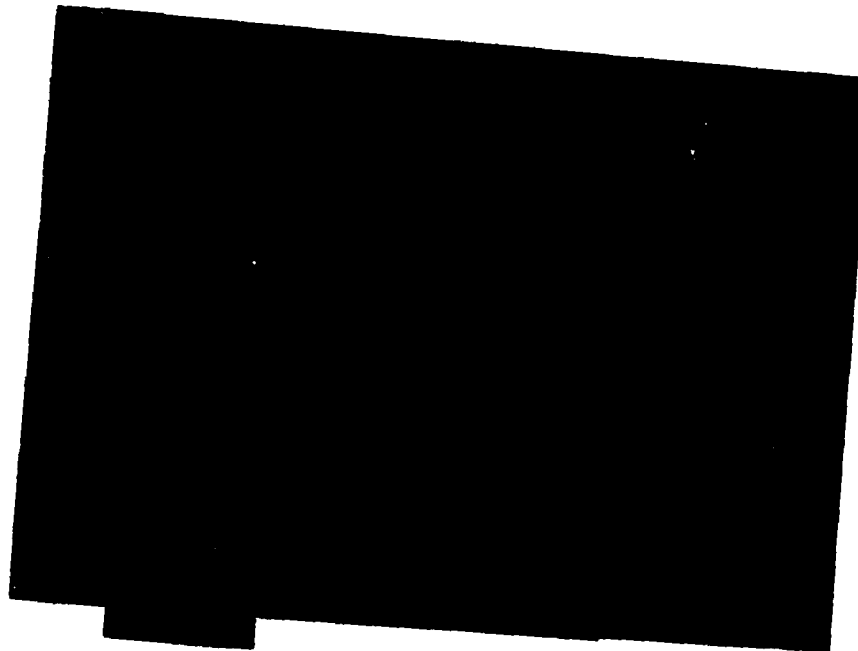


Fig. 4.16 Cross Sectional View of Whisker #1  
(Magnification = 27.5K)

Shape/Striations. The striations running along the length of the whisker are the result of groves or changes in the whisker's shape. This is illustrated in Fig. 4.16 which shows the cross section of Whisker #1.

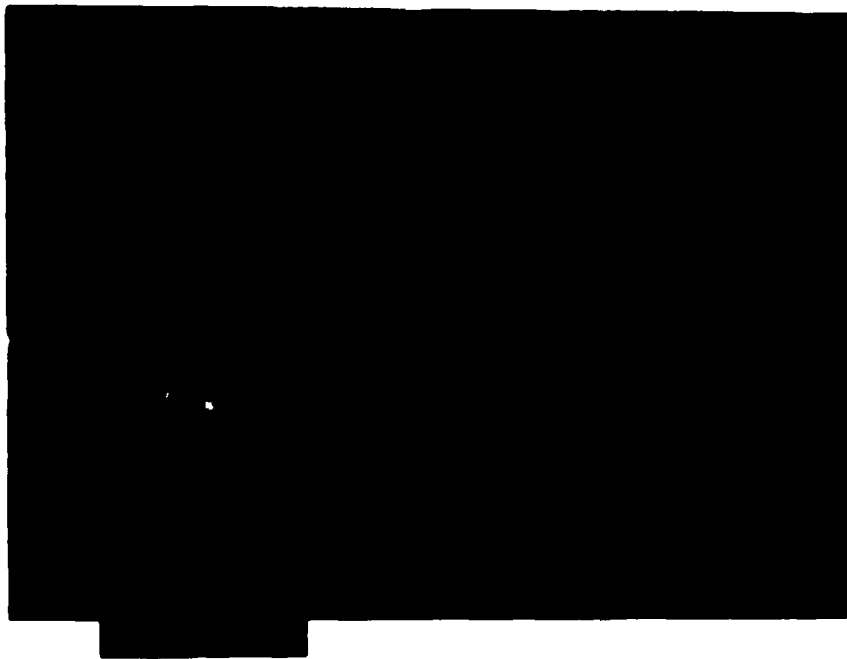


Fig. 4.17 Kinking in Whisker #9  
(Magnification = 21K)

Kinking. Kinking is also present in some of the whiskers as shown in Fig. 4.17. These kinks appear very similar to the ones obtained with thermally grown whiskers.

Nucleation Sites. The whiskers were observed growing out of hillocks and out of the surface of the test stripe. In each case there appears to be some form of mass build up at the base of the whisker. An SEM micrograph of whisker #8 shows a rise in the surface of the stripe around the base of the whisker in Fig. 4.18. A STEM micrograph (Fig. 4.19) confirms that it is an accumulation of mass since the area appears dark. This accumulation of mass may be a hillock which formed under the stripe or recrystallization within the stripe.

None of the whiskers appear to grow out of a grain or out from between grains. The whiskers that do not grow out of hillocks are too large to permit a study of their base. Dr. Blech also stated that the majority of his thermally grown whiskers were too thick to permit a study of the nucleation site structure.

While some of the whiskers emerge from beneath the edge of the test stripe as shown earlier in Fig 4.16, none of the whiskers grow beneath the test stripes. It is also important to note that none of the whiskers penetrated the underlying oxide.

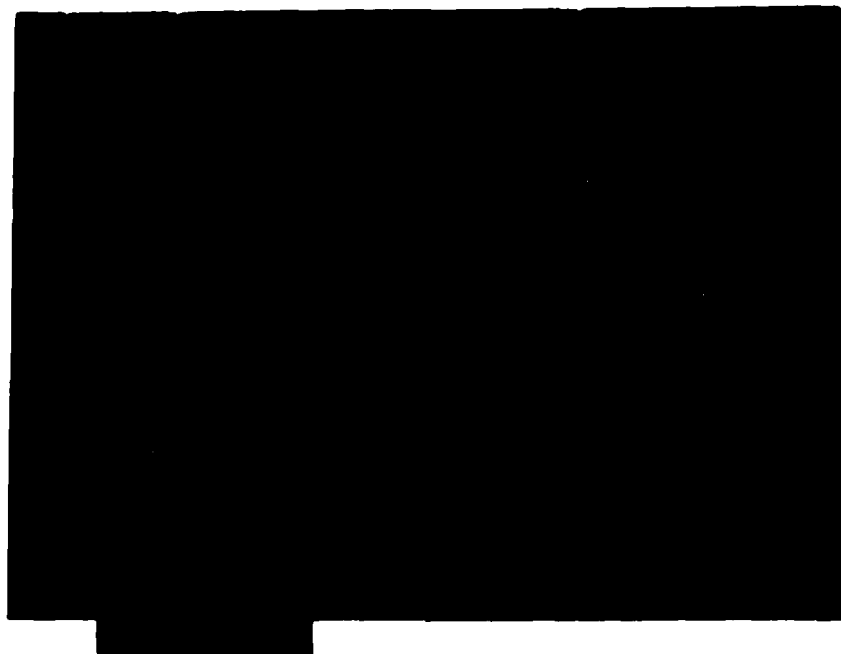


Fig. 4.18 SEM Micrograph of the Swollen Base  
Around Whisker #8 (Magnification = 6.25K)

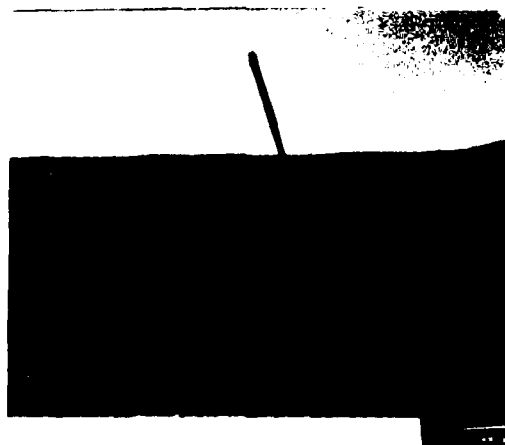


Fig. 4.19 Bright Field Micrograph of Whisker #8  
(Magnification = 17k)

Short Circuit. The threat of short circuits by whiskers is evident from Fig. 4.20. Here Whisker #3 grew until it made contact with the adjacent large stripe. After contact was made, the large current density through the small diameter whisker resulted in Joule heating causing the whisker to burn out like a filament.

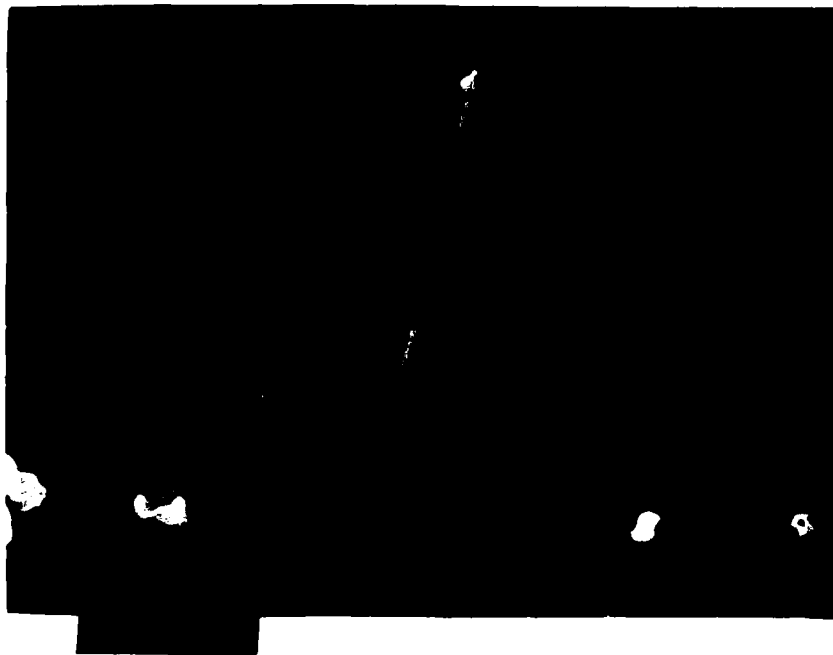


Fig. 4.20 The Remains of Whisker #3 After Creating a Short Circuit With an Adjacent Stripe (Magnification = 2.4K)

### Summary

The static and insitu tests produced over 15 whiskers, twelve of which were selected for analysis. The locations of these whiskers restricted the diffraction analysis to five whiskers. The analysis shows that the crystallographic orientation of all five whiskers is  $\langle 110 \rangle$  which agrees with previous studies on thermally grown whiskers.

A number of morphological observations reveal some interesting characteristics among these whiskers. These observations include internal dislocations, surface structure and striations, kinking, and mass accumulation at all nucleation sites.



## V. Conclusions and Recommendations

### Conclusions

Twelve whiskers were successfully produced by electromigration on suspended aluminum linestrips. Static and in-situ tests were conducted by passing a current density of approximately  $0.45 \times 10^6$  A/cm<sup>2</sup> through the suspended test strips. The resulting whiskers were analyzed using STEMs and SEMs. The results of this analysis are as follows:

1. The crystallographic orientation of aluminum whiskers produced by electromigration is  $\langle 110 \rangle$  along the growth axis. This agrees with previously published orientation results for thermally grown whiskers.

2. Some of the whiskers have internal dislocations. The nature or cause of these dislocations was not determined.

3. The striations running parallel to the whisker are surface grooves or irregularities on the whisker's surface.

4. Some whiskers originate in hillocks. Others appear to protrude out of the aluminum linestripe, but STEM and SEM micrographs reveal mass accumulation at the base of the whisker.

5. The effective length of the suspended stripe in relation to the  $J_c L$  product may be the distance between the thermal gradients along the perimeter of the etched region.

## Recommendations

In the course of performing this research effort, a number of problems were encountered as were new opportunities for further study. This section contains a number of recommendations to improve the testing capability and expand the research.

Test Improvements. The following recommendations are for improvements to testing efficiency and controllability.

1. While it does afford the capability to perform in-situ work within the STEM, the Mark II holder requires additional modifications to improve its efficiency. Bonding is very difficult due to the difference in height between the sample and the holder's bonding pads. A spacer should be designed with a tapered hole to raise the sample without limiting the tilting capability within the microscope.

Another approach which will provide a major increase in efficiency is the design and use of clip-in inserts. The samples would be mounted to the inserts and then placed into the holder. The advantages are easier bonding and fast turn around at the test site. It presently takes two to three days to remove a sample and mount another for testing.

2. The current BTV test stripe and etching procedures present a number of problems in sample preparation. The diameter of the etched region is uncontrollable which results in different characteristics for each test.

A new test pattern consisting of three independent stripes with a common bonding pad should be designed.

Furthermore, a second mask should be designed to mask the back side of the chip for etching. Using Potassium Hydroxide to etch the alignment marks through a <110> wafer before processing the wafers should solve the problem of aligning the two masks (33).

New Research. The following recommendations are for continued studies related to the whiskers produced by electromigration.

1. It is difficult to observe the nucleation process of whiskers since their location cannot be predicted. It is therefore desirable to try to force the whisker to grow in a given location. An artificial stress relief may be created with a small hole in a passivation layer near the anode (25:1205).

2. Since Blech reported that annealed test stripes did not produce any whiskers (3:161) additional studies should be conducted to find out if there is a minimum average grain size required for whiskers to grow. Test stripes could be annealed at varying temperatures and then subjected to dc static testing to determine if a minimum anneal is required to reduce the possibility of whisker growth.

3. Some of the whiskers analyzed during this investigation revealed internal dislocations. Further studies should be conducted to analyze these faults. This may provide valuable information regarding what is happening at the base of the whisker.

4. It is stated in Chapter IV that the large thermal gradients along the perimeter of the etched region establish the effective length of the test stripe. This effective length therefore determines the minimum (critical) current density required to induce electromigration according to the  $J_C L$  product. To show this, tests must be performed on suspended stripes of varying lengths to determine their minimum current density for electromigration. The results of these tests should then be compared to see if  $J_C L$  does equal a constant.

## Appendix A

### Test Pattern Fabrication

This appendix describes the fabrication process used to obtain well defined test patterns, Bridge Test Vehicles, with the required aluminum thickness. It is divided into two major sections, oxidation and metallization.

#### Oxidation

The oxide establishes a buffer region for the etch process. Since the oxide appears transparent under the microscope, it permits the safe removal of the silicon without damaging the aluminum stripes. It is also important to remove excess oxide since its amorphous structure diffracts the electron beam during analysis. A suggested initial thickness is 5000 Å since it provides sufficient protection for the etching process outlined in Appendix B.

The following procedures are provided for producing an oxide layer approximately 5000 Å thick.

Procedures. Prior to oxidation the wafers undergo the following precleaning process to remove particulates, organic residues, and inorganic contaminants.

1. Place the wafers in a 3:2 solution of sulfuric acid and hydrogen peroxide for 15 minutes to remove particulates and organic substances. This mixture produces an exothermic reaction which remains very hot (~ 130 °C) for about 30 minutes.

\*\*\*\*\*

#### CAUTION

The beaker should be placed on a pad to avoid burning or discoloring any underlying surface.

\*\*\*\*\*

2. Rinse the wafers in deionized water (DIW) for 5 minutes.

3. Dip the wafers in a 10:1 solution of DIW:hydrofluoric acid (HF) for 15 seconds to remove the thin oxide produced in steps 1 and 2.

4. Next, rinse the wafers in DIW for five minutes and then spin or blow dry with nitrogen gas.

\*\*\*\*\*

#### WARNING

The acids used are dangerous and will result in burns. Hydrofluoric acid is especially dangerous as it can not be felt or detected until hours later. If contact occurs, rinse heavily with water and report to the hospital.

\*\*\*\*\*

Transport the wafers to the diffusion furnace for oxidation. (Any transportation of the wafer should be in a container to minimize contamination)

The process of introducing the wafers into the oxidation tube, oxidizing, and removing them are as follows:

1. Place the wafers into the oxidation tube near the loading edge. From there, slowly push them in at a rate of one inch per minute for 10 minutes under dry oxidation. This prevents the wafers from warping due to a sudden temperature change.

2. Quickly push the wafers to the center of the tube as wet oxidation is introduced for 50 minutes at 1050 °C.

3. Once that cycle is complete, remove the wafers in the same manner as they were introduced by quickly pulling them to within 10 inches of the entrance. Then slowly remove (one inch per minute) under 10 minutes of dry oxidation.

4. Remove the wafers from the tube and allow them to cool before placing them in a container.

\*\*\*\*\*  
WARNING

The end of the pushrod is very hot when removed from the oven and will result in burns if touched. Wear heat resistant gloves when handling the pushrod.

\*\*\*\*\*  
\*\*\*\*\*  
WARNING

After placing the end cap on the tube, close the outer metal door of the furnace. A sudden change in pressure may blow the cap off of the tube. The end cap is extremely hot and heat resistant gloves must be worn when handling.

\*\*\*\*\*

Since the exact thickness is not critical, the approximate thickness can be verified with a color chart.

### Metallization

Two different metallization processes were used and, to a certain extent, provided satisfactory results. The first method, described in (27:A-3) used a metal etch. While it successfully produced the pattern, the stripes were poorly defined. The second process, the lift off technique, provided improved definition as illustrated in Fig. A.1.

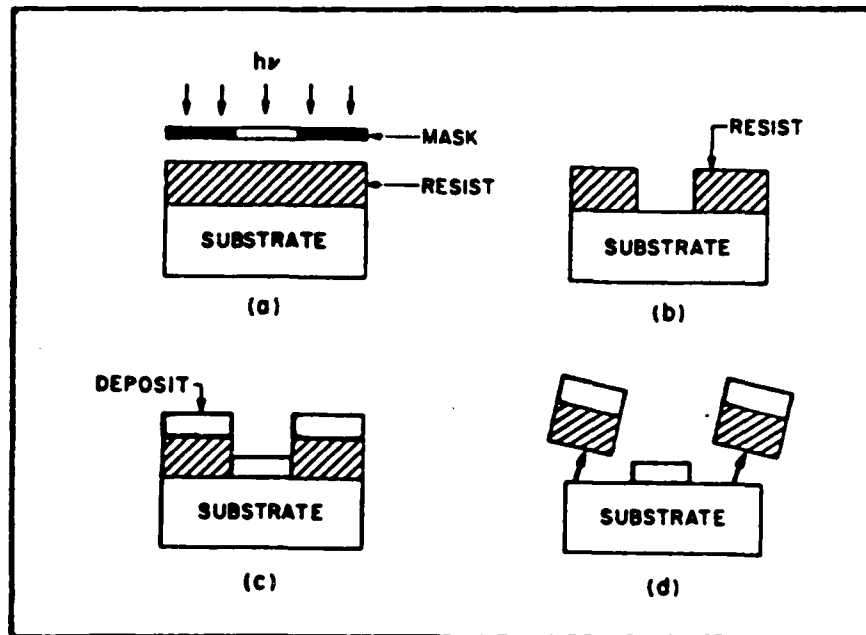


Figure A.1 Lift-off Technique (32:441)

Procedures. The following procedures are used to acquire the desired test patterns.

1. Bake out the wafers at 220 °C for 1 hour to remove moisture.
2. Spin on the positive photoresist at a speed of 5000 rpm for 30 sec.
3. Spin on the adhesion promoter, hexamethyldisilazane (HMDS), at a speed of 5000 rpm for 30 sec.
4. Prebake at 70 °C for 30 min to harden the photoresist.
5. Using a mask aligner, expose the wafers for 70 sec.



6. Develop by gently spraying with Microdeposit 351 Developer for 30 sec followed by a DIW rinse for 30 sec.

7. Inspect for pattern definition. The oxide should be visible between the stripes. If it is not, go back to step 6 and develop for a shorter length of time.

8. Evaporate on aluminum to a thickness of 2000 Å.

9. Remove the excess aluminum by soaking sample in acetone. An ultrasonic bath may be required in the removal process.

10. Use the Dektac to measure the aluminum thickness and ensure that it is not greater than 2000 Å.

11. Scribe the wafer into individual chips.

## Appendix B

### **Producing Suspended Linestripes**

The most important and time consuming factor of suspended stripe experimentation is the etching process. Once the desired stripe is selected, the hole must be masked in the appropriate location with a reasonable diameter. The actual etching process must not only etch away the silicon but also most of the oxide to minimize distortion.

#### Stripe Selection

The Bridge Test Vehicles are first examined in an optical microscope for defects. These defects include shorts, open or fragmented lines, and nicks in the aluminum. Next the test stripes should be probed to ensure electrical continuity.

#### Wax Masking

The following procedures describe the method used to mask a hole on the back of the chip with wax.

1. Turn on the Nucerite hot plate and adjust the dial setting to 105.
2. Place a clean sapphire disk on the hot plate and allow a few minutes for the disk to reach the plate temperature.

3. Place and melt a thin layer of pico-lastic D100 wax on the sapphire disk until it covers an area approximately 1/2" in diameter.

4. Place the chip with the pattern side down on the melted wax and gently press it down into the wax.

5. Using the straight pin, dip the tip into the melted wax and pull it away slowly. If the wax is at the correct temperature a short string of wax can be laid across the back of the chip. Use this method to cover the back of the chip except for the desired hole.

6. Keep the exposed hole as close to the center of the chip as possible. The etchant is isotropic and may undercut and weaken the region under the bonding pads.

7. Place the sapphire disk on a heat sink to promote rapid hardening of the wax.

#### Producing the Suspended Linestripe

The etching process is a repetitive sequencing of etching, rinsing, and inspecting. The silicon etch is a 10:6:6 solution of acetic acid:nitric acid:hydrofluoric acid. Ammonium fluoride is used to stop the etching process by neutralizing the acids and a 10:1 mixture of DIW:HF is used to etch the oxide.

The following process is used to produce a suspended stripe.

1. Dip the sapphire disks into the 10:6:6 solution of acetic acid:nitric acid:hydrofluoric acid for 15 minutes.

Four disks can be etched simultaneously if a solution volume of at least 660 ml is used in the proportion of 300:180:180.

2. Dip the disks into ammonium fluoride for one minute to neutralize the acids.

3. Rinse in DIW for 5 minutes.

\*\*\*\*\*

#### WARNING

The acids used are dangerous and will result in burns. Hydrofluoric acid is especially dangerous as it can not be felt or detected until hours later. If contact occurs, rinse heavily with water and report to the hospital.  
\*\*\*\*\*

4. Inspect the etched region with an optical microscope to determine if the test stripes are visible. If they are not, repeat step one for a reduced amount of time.

If the remaining silicon is very thin, the outline of the test stripes can be seen by transmitting light up through the sample.

5. Dip the disk in 10:1 DIW:HF for 10 sec to etch the oxide.

6. Repeat steps 2, 3, and 5 until the thickness of the oxide is reduced.

7. Remove the wax by soaking the disk in acetone for overnight. Remove the chip and gently spray with acetone to remove any remaining wax. Then rinse with methanol followed by DIW.

8. Inspect the test stripe again for continuity.

## Appendix C

### Thermal Model of a Suspended Linestripe

Electromigration testing with suspended aluminum linestripes can result in significant Joule heating (13:1410,1412). This results in high temperatures in the center of the stripe, and increased thermal gradients along the etched perimeter which accelerate the electromigration process (5:487). It is, therefore, necessary to establish the thermal profile for a suspended linestripe.

The suspended stripe is modeled in one dimension as a current carrying wire with heat sinks at both ends (7:364). The model establishes the thermal profile according to (7:364-365)

$$T(x) = 1/\beta \{ [|\cos a(\xi - x)| / \cos(a\xi)] - 1 \} + T_0 \text{ (}^\circ\text{C)} \quad (\text{C.1})$$

and

$$a^2 = \beta p_0 J^2 / K \quad (\text{cm}^{-2}) \quad (\text{C.2})$$

where

- $x$  = distance along the length of the stripe (cm)
- $\beta$  = temperature coefficient of electrical resistivity ( $^\circ\text{K}^{-1}$ )
- $\xi$  = one half the length of the suspended stripe ( $L/2$ )
- $p_0$  = the electrical resistivity at  $0^\circ\text{C}$  ( $\Omega\text{-cm}$ )
- $T_0$  = the temperature of the stripe at each end ( $^\circ\text{C}$ )
- $K$  = thermal conductivity coefficient ( $\text{W/cm-}^\circ\text{K}$ )
- $J$  = current density ( $\text{A/cm}^2$ )

With the values,

$$\begin{aligned}\beta &= 0.004 \text{ } (^{\circ}\text{K}^{-1}) & (7:365) \\ p_0 &= 3.1 \text{ at } 0 \text{ } ^{\circ}\text{C} \text{ } (\mu\Omega\text{-cm}) & (7:365) \\ K &= 2.04 \text{ } (\text{W/cm}^{\circ}\text{K}) & (33:11) \\ T_0 &= 23 \text{ } (^{\circ}\text{C}) \\ J &= 0.5 \times 10^6 \text{ } (\text{A/cm}^2)\end{aligned}$$

the maximum temperature for the center of the stripe ( $x = \xi$ ) is calculated using Eq (C.1) for various values of  $L$  and displayed in Fig. C.1. The melting temperature for aluminum is  $660 \text{ } ^{\circ}\text{C}$ . Therefore, the length of the suspended stripe should be limited to approximately  $300 \text{ } \mu\text{m}$  to stay well below the melting point of aluminum.

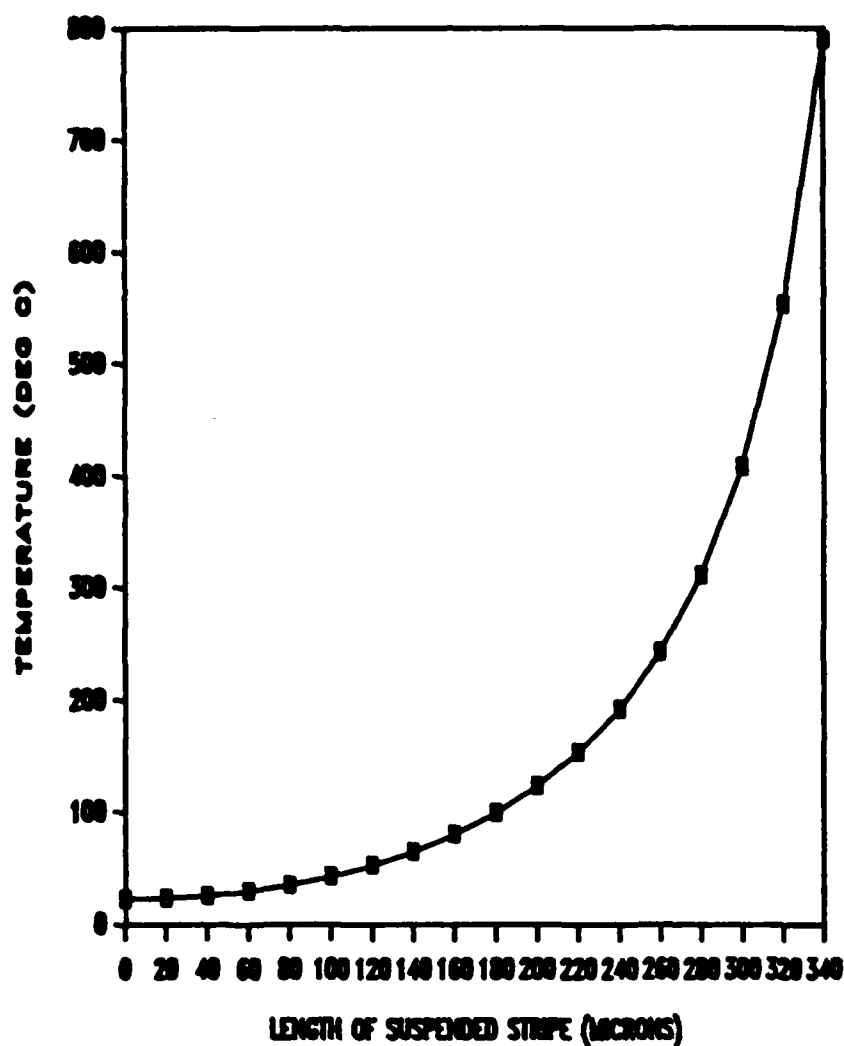


Fig. C.1 Maximum Temperature at the Center of the Stripe for  $J = 0.5 \times 10^6 \text{ A/cm}^2$

Thermal Profile. The thermal profile for the suspended linestripe is also calculated using Eq (C.1). The normalized thermal profile for a suspended linestripe 200  $\mu\text{m}$  long, 10  $\mu\text{m}$  wide, and 1550  $\text{\AA}$  thick with a current density of  $0.5 \times 10^6 \text{ A/cm}^2$  is depicted in Fig. C.2.

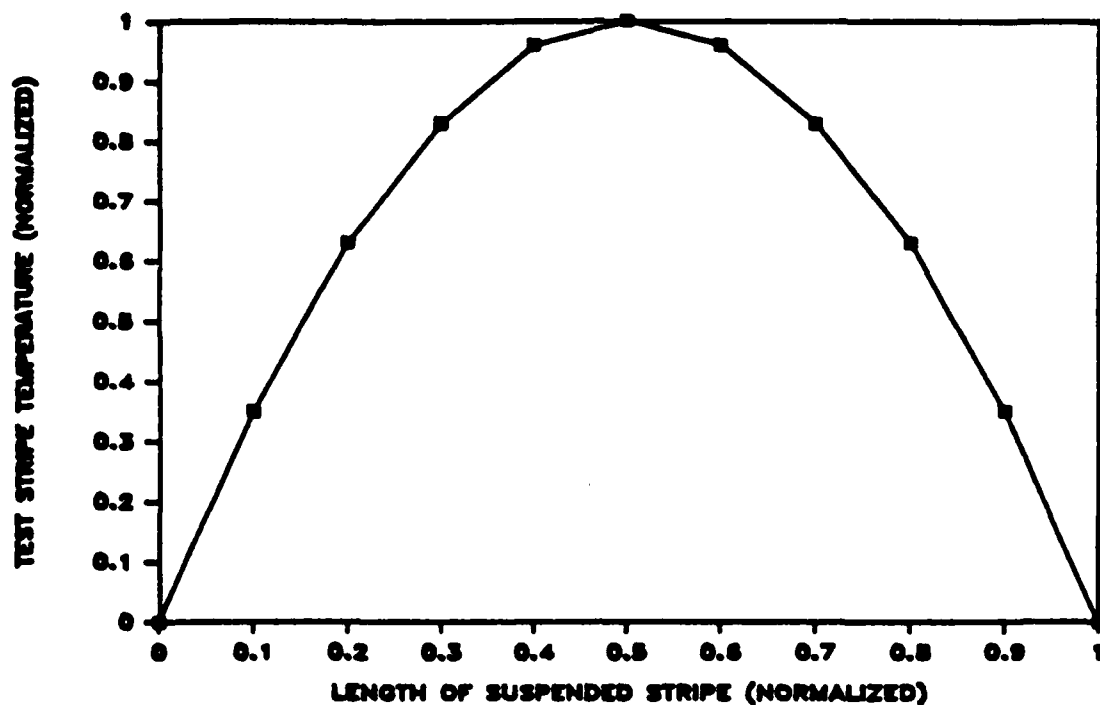


Fig. C.2 Normalized Thermal Profile for a Suspended Linestripe

The maximum temperature for this curve is easily found from Fig. C.1 for  $L = 200 \mu\text{m}$ . The values are normalized to provide a generalized profile of the linestripe. From Eq (C.1), the thermal gradient  $\partial T / \partial x$  is given by

$$\partial T / \partial x = 250 \{ a [ |(\tan a\xi)(\cos ax) - \sin ax| ] \} \quad (\text{C.3})$$

The maximum temperature gradient occurring at the perimeter for a range of suspended linestripe lengths is calculated using Eq (C.4) and displayed in Fig. C.3.



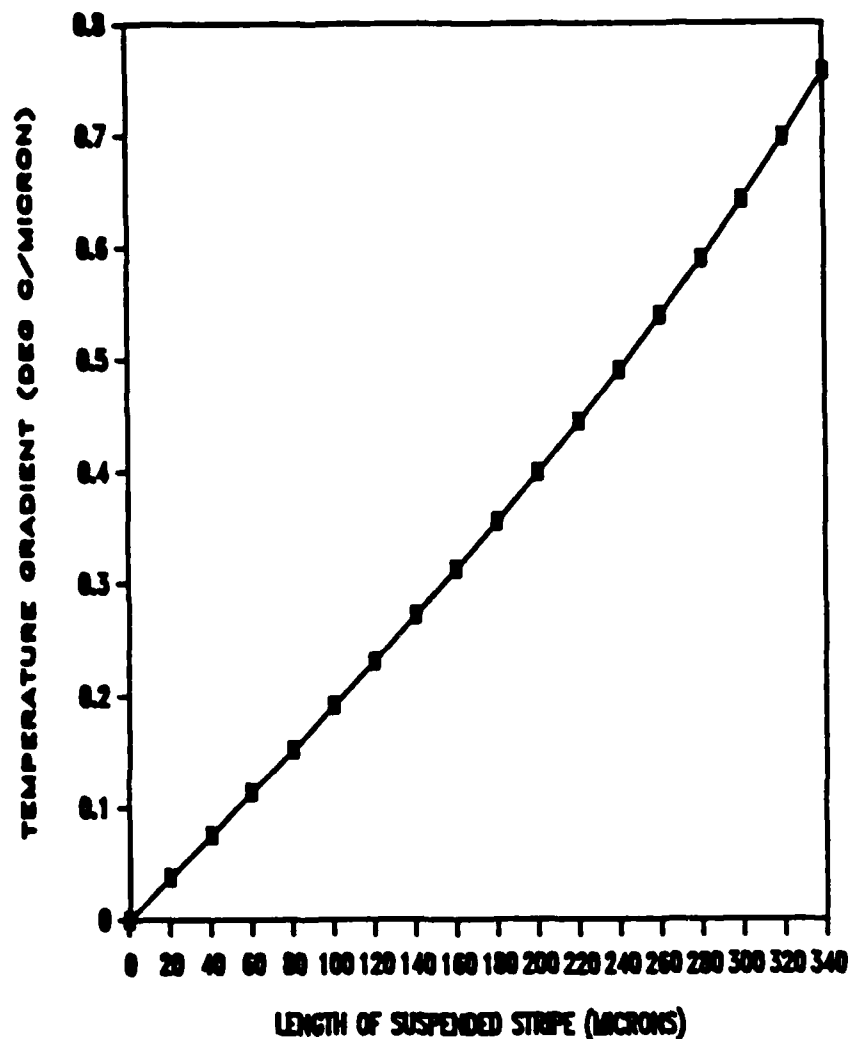


Fig. C.3 Maximum Temperature Gradient as a Function of Length for  $J = 0.5 \times 10^6$  A/cm<sup>2</sup>

The corresponding normalized thermal gradient curve is shown in Fig. C.4. As discussed earlier, the maximum temperature gradient occurs along the perimeter of the etched region. The temperature gradient at any point of a suspended linestripe is obtained from Fig. C.3 and C.4.

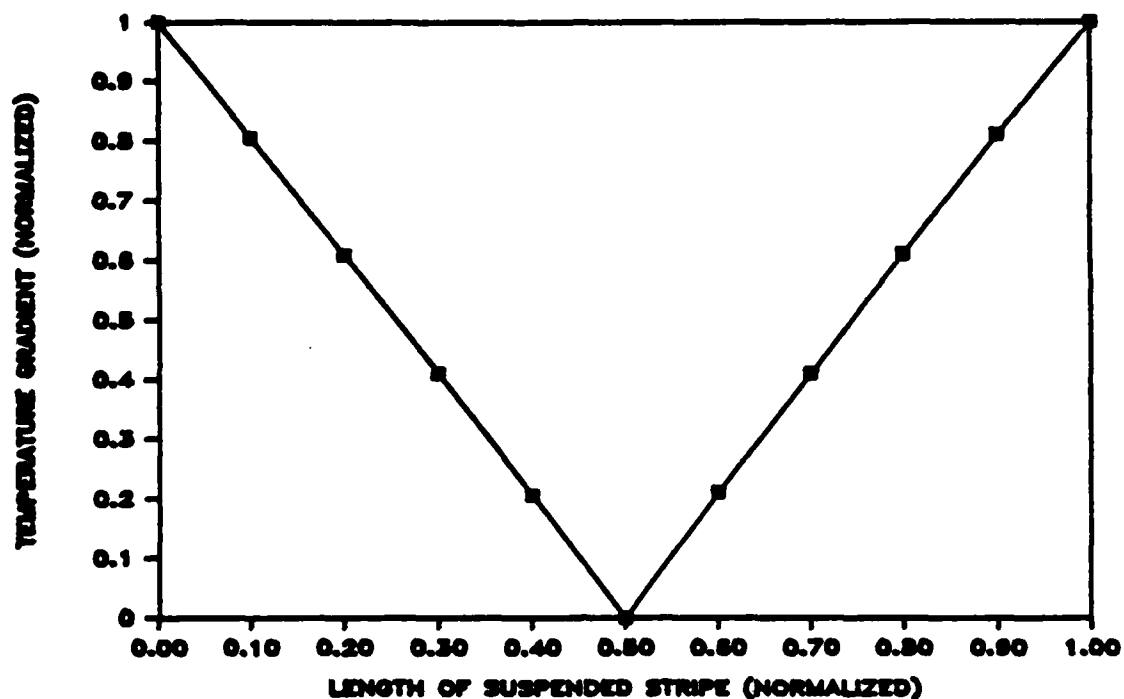


Fig. C.4 Normalized Graph of the Temperature Gradient for Suspended Linestripes (Normalization factor  $L = 200 \mu\text{m}$ )

The temperature of the aluminum stripe over the un-etched portion of the chip ( $T_0$ ) was determined using the model depicted in Fig. C.5 (19:26).

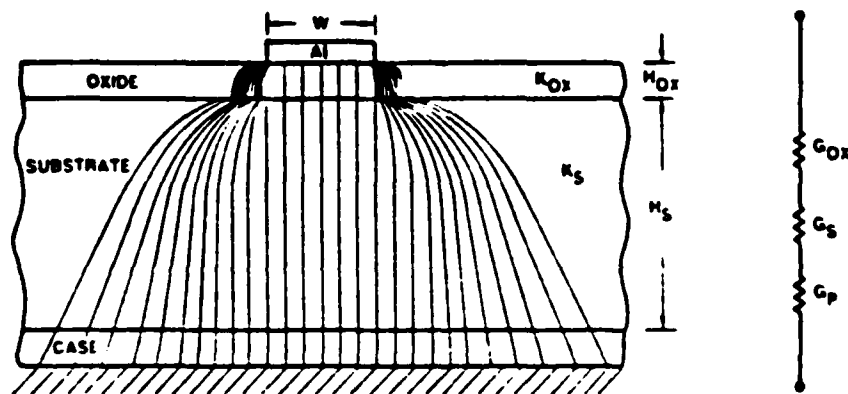


Fig. C.5 Thermal Conductance Model (19:26)

The increase in temperature ( $\Delta T$ ) within the stripe is calculated from the following equations (19:25)

$$I^2 R = G_T \Delta T \quad (W) \quad (C.4)$$

$$1/G_T = 1/G_{OX} + 1/G_S + 1/G_P \quad (W/^{\circ}K) \quad (C.5)$$

$$G_{OX} = k_{OX} L [W + \Delta W_{OX}] / H_{OX} \quad (W/^{\circ}K) \quad (C.6)$$

$$G_S = k_S L (W + \Delta W_S + \Delta W_{OX}) / H_S \quad (W/^{\circ}K) \quad (C.7)$$

$$\Delta W = 0.44(H) \quad (cm) \quad (C.8)$$

where

$I$  = electric current (A)  
 $R$  = resistance of the test stripe ( $\Omega$ )  
 $G_T$  = thermal conductance of the total path (W/ $^{\circ}K$ )  
 $G_{OX}$  = thermal conductance of the oxide (W/ $^{\circ}K$ )  
 $G_S$  = thermal conductance of the substrate (W/ $^{\circ}K$ )  
 $G_P$  = thermal conductance of the package (W/ $^{\circ}K$ )  
 $k_{OX}$  = thermal conductivity of the oxide (W/cm- $^{\circ}K$ )  
 $k_S$  = thermal conductivity of the substrate (W/cm- $^{\circ}K$ )  
 $W$  = width of the conductor (cm)  
 $L$  = length of the conductor (cm)  
 $\Delta W$  = additional width adjustment for thermal flux through the edges (cm)  
 $H_{OX}$  = thickness of the oxide (cm)  
 $H_S$  = thickness of the substrate (cm).

The conductance of the package is neglected since both the Mark II holder and the TO-5 header provide excellent heat sinks. By substituting the following values of

$I$  = 6.19 mA  
 $R$  = 92.25  $\Omega$   
 $k_{OX}$  = .014 W/cm- $^{\circ}K$  (34:852)  
 $k_S$  = 1.5 W/cm- $^{\circ}K$  (34:851)  
 $L$  = 957  $\mu m$   
 $W$  = 7.5  $\mu m$   
 $H_{OX}$  = 5000  $\text{\AA}$   
 $H_S$  = 229  $\mu m$

the increase in the stripe temperature is less than 1  $^{\circ}C$ .

Dr. Blech also states that the unetched portion of the stripe remains at "ambient temperature" (5:486).

The accuracy of this model was not determined in this thesis effort; however, it has been used in (5) and (7).

## Appendix D

### AC Tests

The presence of large thermal gradients in suspended linestripes raises a question about the influence of thermal migration. One method of testing for the presence of thermal migration requires a 60 Hz ac source (13:1410,14:23). The ac test is designed to create the same thermal conditions within the stripe which occur during the electromigration tests. By obtaining an ac rms current equal to the current level used in dc tests, equivalent joule heating occurs without net current flow. The current changes direction during each half cycle. If voiding or accumulation does not occur during the ac test, the possibility of thermal migration is eliminated.

This appendix describes the configuration of the test equipment, the testing procedures, and the results.

#### Test Equipment

The test equipment is connected as illustrated in Fig. D.1. The sine wave generator is a Wavetek Voltage Controlled Generator (VCG) Model III, the oscilloscope is a Tektronix Type 453 Oscilloscope, and the ammeter is a Fluke 8010A Digital Multimeter.

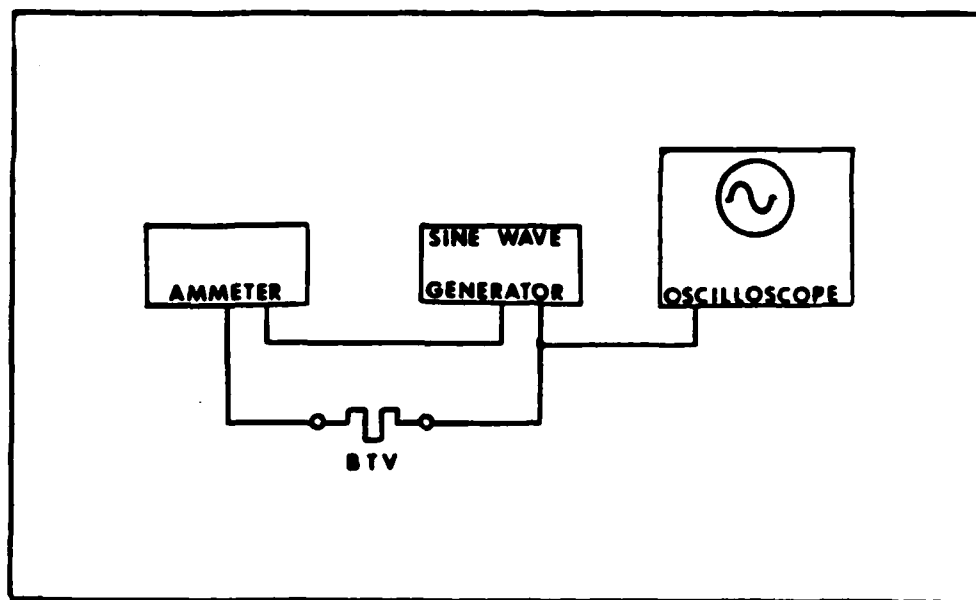


Fig. D.1 AC Test Equipment

### Test Procedure

The following procedures are used to conduct the ac test.

1. Place the TO-5 header with a mounted test stripe into the vacuum box and reduce the pressure to two torr.
2. With the test stripe disconnected, adjust the VCG to produce a 60 Hz sine wave on the oscilloscope.
3. Reduce the amplitude before connecting the test stripe and set the ammeter for RMS current reading.

4. Connect the test stripe and increase the signal amplitude until the desired rms current is obtained.

5. Record the starting time.

6. After the desired test time has passed, assuming no failure, turn down the VCG amplitude and disconnect the test stripe.

7. Transfer the sample to the SEM or STEM and examine it for any signs of thermal migration. Thermal migration will cause voiding in the conductor's center and accumulation at both the cathode and anode side of the etched region.

If thermal migration has not occurred, the sample may be subjected to equivalent dc current for comparison purposes.

#### Results of AC Testing

Three ac test were conducted with inconclusive results. While thermal migration did occur, the test stripe configuration was different than that used to generate whiskers for this thesis. An example of the thermal migration is shown in Fig. D.2. An rms current density of  $0.45 \times 10^6$  A/cm<sup>2</sup> was passed through the 332  $\mu$ m suspended stripe. Failure occurred in less than two hours. The voiding in the center (A) and the hillock formation on each side (B) indicates thermal migration.

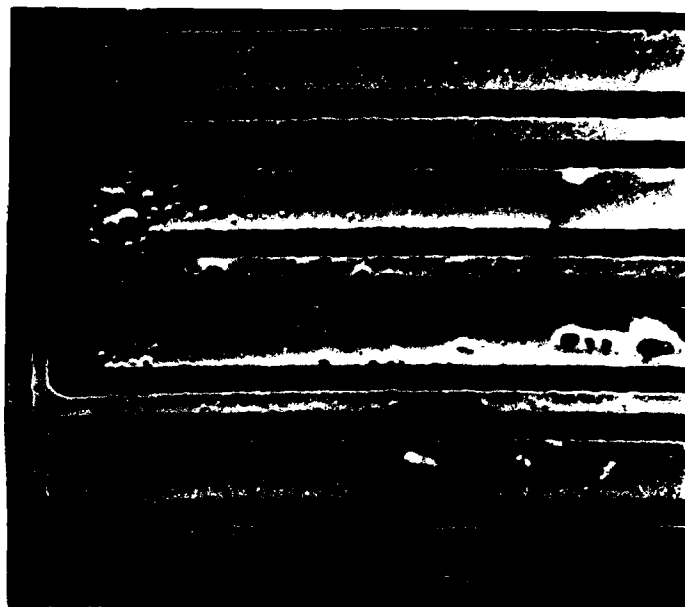


Fig. D.2 Thermal Migration (Magnification = 1K)

The test results are inconclusive because of the bend in the stripe on each side of (A). The resulting current crowding and changes in the thermal profile at these bends render the results unreliable and inconclusive.

Two other experiments were also performed with the same configuration and inconclusive results. .



## Bibliography

1. Towner, Janet M. "Electromigration-Induced Short Circuit Failure," 23rd Preceedings IEEE Reliability Physics, 81-86 (1985).
2. Lloyd, J.R. "Electromigration-Induced Extrusions in Multi-Level Technologies," 21st Annual IEEE IRPS, 208-210 (1983).
3. Blech, I.A., P.M. Petroff, K.L. Tai, and V. Kumar "Whisker Growth in Al Thin Films," Journal of Crystal Growth, 32: 161-169 (1975).
4. Blech, I.A. and E.S. Meieran "Direct Transmission Electron Microscope Observation of Electrotransport in Aluminum Thin Films," Applied Physics Letters, 11 (8): 263-266 (October 1967).
5. Blech, I.A. and E.S. Meieran "Electromigration in Thin Al Films," Journal of Applied Physics, 40 (2): 485-491 (February 1969).
6. Horowitz, S.J. and I.A. Blech "Electromigration in Al/Cu/Al Films Observed by Transmission Electron Microscopy," Materials Science and Engineering, 10: 169-174 (1972).
7. Va'vra, I., P. Lobotka, F. Zachar and J. Osvald "TEM In-Situ Observation of Electromigration Damage in Al-Cu Strips," Physica, 63: 363-370 (1981).
8. Black, James R. "Electromigration--A Brief Survey and Some Recent Results," IEEE Transactions on Electron Devices, ED-16: 338-347 (April 1969).
9. Ames, I., F.M. d'Heurle and R.E. Horstman "Reduction of Electromigration in Aluminum Films by Copper Doping", IBM Journal of Research and Development, 14: 461-463 (July 1970).
10. Kinsbron, E. "A Model for the Dependence of Electromigration Lifetimes in Aluminum Thin-Film Stripes," Applied Physics Letters, 36: 968-970 (June 1980).
11. Girifalco, L.A. Atomic Migration in Crystals. New York: Blaisdell Publishing Company, 1964.
12. Black, James R. "Physics of Electromigration," 12th Annual Proceedings on Reliability Physics, 142-147 (1974).

13. D'Heurle, Francois M. "Electromigration and Failure in Electronics: An Introduction," Proceedings of IEEE, 59: 1409-1417 (October 1971).
14. Hummel, R.E. and H.B. Huntington "Electro- and Thermo-transport in Metals and Alloys," Proceedings of the Metallurgical Society of AIME and the American Society of Metals Symposium. 1-5, University of Microfilms International, Michigan, (1986).
15. Schrieber, H.-U "Activation Energies for the Different Electromigration Mechanisms in Aluminum," Solid State Electronics, 24: 583-589 (1981).
16. Laudice, R.A. The Growth of Single Crystals. New Jersey: Prentice-Hall Inc, 1970.
17. Richards, B. P. and P. K. Footner "Morphological Aspects of Electromigration," GEC Journal of Research, 1: 1-19 (1984).
18. Lloyd, J.R. "Electromigration," Journal of Metals, 36 (7): 54-56 (July 1984).
19. Wu, C.J. and M.J. McNutt "Effects of Substrate Thermal Characteristics on the Electromigration Behavior of Al Thin Film Conductors," IEEE IRPS, 24-31 (1983).
20. Hershkovitz, M., I.A. Blech, and Y. Komen "Stress Relaxation in Thin Aluminum Films," Thin Solid Films, 130: 87-93 (1985).
21. Blech, I.A. and C. Herring "Stress Generation by Electromigration," Applied Physics Letters, 29: 131-133 (August 1976).
22. Sinha, A.K. and T.T. Sheng "The Temperature Dependence of Stresses in Aluminum Films on Oxidized Silicon Substrates," Thin Solid Films, 48: 117-126 (1978).
23. Garosshen, T.J., Stephenson, T.A. and T.P. Slavin "Aluminum Metallization Technology for Semiconductor Devices," Journal of Metals, 37 (5): 55-59 (May 1985).
24. Blech, I.A., Telephone Interview. Zoran Corp., Santa Clara, CA, 24 June 1986.
25. Blech, I.A. "Electromigration in Thin Aluminum Films on Titanium Nitride," Journal of Applied Physics, 47: 1203-1208 (April 1976).

26. Blech, I.A. and K.L. Tai "Measurement of Stress Gradients Generated by Electromigration," Applied Physics Letters, 30: 387-389 (April 1977).

27. Maskowitz, Capt James V. and Capt William E. Rhoden Electron Microscopy Observation of Electrotransport. MS Thesis, AFIT/GE/ENG/85D-77. School of Engineering, Air Force Institute of Technology (AU), Wright-Patterson AFB OH, December, 1985 (AD-25).

28. Catalog No. 1034-1035 Aluminum Diffraction Standard. Ernest F. Fullum, Inc. New York, 1977.

29. Edington, J.W. Practical Electron Microscopy in Materials Science. New York: Van Nostrand Reinhold Company, 1976.

30. Morris, R.B. and W. Bonfield "The Crystallography of  $\alpha$  - Tin Whiskers," Scripta Metallurgica, 8: 231-236 (1974).

31. Mainger, Capt Bob., AFIT Student. Personal Interview. AFIT, Wright-Patterson AFB OH, 1 October 1986.

32. Sze, S.M. Semiconductor Devices Physics and Technology. New York: John Wiley & Sons, 1985.

33. Kreith, Frank and W.Z. Black. Basic Heat Transfer. New York: Harper & Row Publishers, 1980.

34. Sze, S.M. Physics of Semiconductor Devices. New York: John Wiley & Sons, 1981.

VITA

Captain Scott L. Linder was [REDACTED] in [REDACTED]. He graduated from [REDACTED] [PII Redacted] in 1973 and later enlisted in the Air Force in 1977. He attended the University of South Carolina through the Airman's Education and Commissioning Program and received the degree of Bachelor of Science in Engineering in December 1981. From there he attended Officer Training School and recieved his commission in April 1982. He served as lead engineer on the AN/ALR-62 Radar Warning Receiver Update Program until he entered the School of Engineering, Air Force Institiute of Technology, in June 1985.

Permanent Address: [REDACTED]  
[REDACTED] [REDACTED]

[PII Redacted]

A172383

## REPORT DOCUMENTATION PAGE

Form Approved  
OMB No. 0704-0188

1a. REPORT SECURITY CLASSIFICATION Unclassified			1b. RESTRICTIVE MARKINGS		
2a. SECURITY CLASSIFICATION AUTHORITY			3. DISTRIBUTION / AVAILABILITY OF REPORT Approved for public release; distribution unlimited		
2b. DECLASSIFICATION / DOWNGRADING SCHEDULE					
4. PERFORMING ORGANIZATION REPORT NUMBER(S)  AFIT/GE/ENG/86D-35			5. MONITORING ORGANIZATION REPORT NUMBER(S)		
6a. NAME OF PERFORMING ORGANIZATION School of Engineering Air Force Institute of Tech-		6b. OFFICE SYMBOL (If applicable) AFIT/ENG	7a. NAME OF MONITORING ORGANIZATION		
6c. ADDRESS (City, State, and ZIP Code) Wright-Patterson AFB, Ohio 45433			7b. ADDRESS (City, State, and ZIP Code)		
8a. NAME OF FUNDING / SPONSORING ORGANIZATION RADC		8b. OFFICE SYMBOL (If applicable) RADC/RBE	9. PROCUREMENT INSTRUMENT IDENTIFICATION NUMBER		
8c. ADDRESS (City, State, and ZIP Code) Griffiss AFB, New York 13441			10. SOURCE OF FUNDING NUMBERS		
			PROGRAM ELEMENT NO.	PROJECT NO.	TASK NO.
			WORK UNIT ACCESSION NO.		
11. TITLE (Include Security Classification) The Characterization Of Whiskers Produced By Electromigration On Suspended Aluminum Linestripes					
12. PERSONAL AUTHOR(S) Scott L. Linder Captain, USAF					
13a. TYPE OF REPORT MS Thesis		13b. TIME COVERED FROM _____ TO _____		14. DATE OF REPORT (Year, Month, Day) 86/December/8	
				15. PAGE COUNT 116	
16. SUPPLEMENTARY NOTATION					
<p style="text-align: right;">Approved for public release; LAW AFR 180-77. Wynn E. WOLAVER 7 April 87 Dean for Research and Professional Development Wright-Patterson AFB OH 45433</p>					
17. COSATI CODES			18. SUBJECT TERMS (Continue on reverse if necessary and identify by block number)		
FIELD	GROUP	SUB-GROUP	Electromigration, Aluminum Whiskers Metal Films, STEM		
14	04				
07	04				
19. ABSTRACT (Continue on reverse if necessary and identify by block number)					
<p>Studies have shown that aluminum whiskers resulting from electromigration are as threatening to device reliability as void formation. However, comparatively little research has been conducted to study their morphology or formation. This study generates whiskers on suspended aluminum test stripes. The aluminum is evaporated onto 9 mil thick silicon wafers with a 5000Å layer of thermally grown silicon dioxide. Normal photolithography techniques are used to produce serpentine test patterns. The silicon substrate is chemically etched to produce aluminum stripes suspended on a thin layer of silicon dioxide. A current density of approximately <math>0.45 \times 10^6</math> A/cm<sup>2</sup> is applied to induce electromigration. The whiskers are examined with a Cambridge MK II Scanning Electron Microscope and analyzed with a JEOL 2000FX Scanning Transmission Electron Microscope. (continued on reverse)</p>					
20. DISTRIBUTION / AVAILABILITY OF ABSTRACT <input type="checkbox"/> UNCLASSIFIED/UNLIMITED <input checked="" type="checkbox"/> SAME AS RPT <input type="checkbox"/> DTIC USERS			21. ABSTRACT SECURITY CLASSIFICATION Unclassified		
22a. NAME OF RESPONSIBLE INDIVIDUAL Donald R. Kitchen, Instructor			22b. TELEPHONE (Include Area Code) (513) 255-4960		22c. OFFICE SYMBOL AFIT/ENG

Block 19. continued

The results of the analysis show that aluminum whiskers grow in a  $\langle 110 \rangle$  direction along the crystal axis. Additional morphological observations reveal internal dislocations and mass accumulation beneath the stripe surface at the whisker's nucleation site.